AD 701 939

THE MILLSTONE HILL PROPAGATION STUDY

John V. Evans

Massachusetts Institute of Technology
Lexington, Massachusetts

26 September 1969

AD 701939

CLEARINGHOUSE
FOR FEDERAL SCIENTIFIC AND TECHNICAL INFORMATION

Distributed . . . 'to foster, serve and promote the nation's economic development and technological advancement.'

U.S. DEPARTMENT OF COMMERCE/National Bureau of Standards

This document has been approved for public release and sale.

MASSACHUSETTS INSTITUTE OF TECHNOLOGY

LINCOLN LABORATORY

THE MILLSTONE HILL PROPAGATION STUDY

J. V. EVANS, Editor

Group 21

TECHNICAL NOTE 1969-51

26 SEPTEMBER 1969

This document has been approved for public release and sale;
its distribution is unlimited.

LEXINGTON MASSACHUSETTS

The work reported in this document was performed at Lincoln Laboratory, a center for research operated by Massachusetts Institute of Technology. The work is sponsored by the Office of the Chief of Research and Development, Department of the Army; it is supported by the Advanced Ballistic Missile Defense Agency under Air Force Contract AF 19(628)-5167.

This report may be reproduced to satisfy needs of U.S. Government agencies.

ABSTRACT

Defensive radar systems for detecting and locating ballistic missiles must be designed to combat the degradation in system performance that can result from atmospheric and ionospheric refraction effects, clutter and scintillation. These phenomena become increasingly severe at low elevation angles and for high latitude stations there is a broad azimuthal sector where the effects are especially severe owing to the very irregular nature of the polar ionosphere and the presence of the aurora.

A program of measurements and data analysis is in progress, primarily centered at the Millstone Hill radar facility, designed to evaluate tropospheric and ionospheric effects on radar measurements capability, with emphasis upon disturbed ionospheric conditions (e.g., when radio aurorae exist). The work is being undertaken jointly by staff members of the Lincoln Laboratory and the Bell Telephone Laboratories. Emphasis in these measurements will be on attempting to separate and characterize the ionospheric and tropospheric components of refraction and scintillation. In order to do this, a UHF lobe-comparison satellite-beacon tracking capability is being added to the precise L-band tracking radar at Millstone. This will permit simultaneous dual-frequency measurements of angle-of-arrival, amplitude and phase fluctuations for paths traversing the polar ionosphere as well as in other directions less subject to propagation effects.

Accepted for the Air Force
Franklin C. Hudson
Chief, Lincoln Laboratory Office

CONTRIBUTORS

J. H. Chisholm

R. K. Crane

J. V. Evans (editor)

A. Freed

M. A. Gordon

J. L. Mann

J. M. Moran

R. E. Newell

R. J. Riley

P. B. Sebring

M. L. Stone

Contents

1. Introduction 1

2. Objectives of the Program 3

A) General 3
B) Phase I 4
C) Phase II 12

3. Review of Atmospheric and Ionospheric Refraction 14

A) Introduction 14
B) The Lower Atmosphere 14
C) Refraction in the Lower Atmosphere 16
D) The Ionosphere 19

i) General 19
ii) Sporadic E 21
iii) Spread F 23
iv) Travelling Ionospheric Disturbances 23

E) Refraction by the Whole Ionosphere 25
F) Effects of Large Scale Irregularities 27
G) Effects of Small Scale Irregularities 27

i) Observations 27
ii) Phase Scintillations 28
iii) Amplitude Scintillations 30
iv) Angular Scintillation 31

4. Review of Radio Auroral Echo Phenomena 34

A) Introduction 34
B) Spatial Distribution and Time Dependence 35
C) Wavelength Dependence 41
D) Observed Velocities 42
E) Theoretical Interpretation 42

5. UHF Refraction Experiment 46

A) Plan 46

i) General 46
ii) Systematic Pointing Errors 46
iii) L-band Active Tracking of Satellites 47

B) Monopulse Error Tracking Calibration 51
C) UHF/L Band Tracking System 54
D) UHF/L Band Observations 59
E) Dispersive Doppler Experiment 61
F) Theoretical and Analytical Study of Refraction 63

i) Improved Models for Tropospheric Refraction 63
ii) Analysis of the Ottawa Trough 65
iii) Secede III Refraction Experiment 65
iv) Equatorial Scintillations 65

6. Auroral Studies 68

A) Introduction 68
B) Test of the Two-Stream Instability Theory 69

i) General 69
ii) Electron Concentration 70
iii) Electric Field 71
iv) Magnetic Field 72
v) Particle Temperatures 72
vi) Neutral Winds 72

C) Future Work 73

i) Scientific Requirements 73
ii) The New Data-Taking Procedure 74
iii) UHF Surveillance 75
iv) Satellite Probing 76
v) Field Orientation Computations 77

1. Introduction

Radiowave propagation through the atmosphere and the ionosphere has been the subject of considerable experimental and theoretical investigation during the last 50 years. The amplitude, phase, bearing and time of arrival of signals reaching the ground are all to some degree altered by the presence of the earth's ionosphere and atmosphere. These effects depend upon choice of frequency, path and the characteristics of the atmosphere and ionosphere in ways which are well understood, yet often hard to predict owing to the considerable variability encountered. This is especially true for paths that traverse the polar ionosphere which is known to be extremely irregular even during magnetically quiet periods. (for example see Nishida 1967)

The irregular nature of the polar ionosphere is believed to be the consequence of a number of factors, viz. the reduced control provided by the sun at high latitudes, the ionization created by precipitation of high energy particles injected from the tail of the earth's magnetosphere, and the open nature of the field lines which allows light ions (H^+ and H_e^+) to escape.

Small scale irregularities occur in the F region which give rise to scintillation of signals passing through. These irregularities have long been recognized as especially intense in auroral regions (and over the equator at night). The morphology of this phenomenon has been widely studied by observing amplitude fluctuations, but unfortunately little work has been done to measure the associated angle-of-arrival (or phase) fluctuations.

During magnetically disturbed conditions an intense electric current system is set up at altitudes near 105 km which can give rise to radar reflections. This is termed the radio aurora (see for example Hultquist and Egeland 1964 or Forsyth 1968). Visual auroral ionization is also present and may give rise to large refraction effects (e.g. Fremouw and Lansinger 1968).

Other propagation effects encountered in polar regions include the polar 'blackout' which is a marked increase in VHF radio wave absorption caused by precipitation of energetic solar protons following some intense flares.

This report outlines a program of study of propagation at UHF and L-band being conducted at the M.I.T. Lincoln Laboratory Millstone Hill radar. The work is being undertaken jointly by staff members of Lincoln Laboratory and the Bell Telephone Laboratories. The section which follows sets forth the principal objectives of the program and the two phases in which the work shall be accomplished. Scientifically the work divides into two main study areas -- refraction effects both in the neutral atmosphere and the ionosphere and the phenomenon of the radio aurora. Brief reviews of these topics are presented in Sections 3 and 4. The work to be carried out in these two areas is discussed in some detail in Sections 5 and 6.

2. Objectives of the Program

A. General

Here we discuss the principal objectives of the work being undertaken at Millstone Hill. These may be summarized as:

(1) to improve the practical understanding of low angle propagation and clutter phenomena in an auroral environment and permit the performance of defensive radar systems to be predicted for such conditions;

(2) to provide, where possible, guidelines for defensive radar improvements and advanced system concepts so that undesirable effects of propagation phenomena may be minimized;

(3) to provide additional basic information on and improved theoretical models of the troposphere and ionosphere under normal and disturbed conditions.

Multi-frequency observations of satellite signals at low elevations have been made (e.g. Hughes et al. 1964) which permitted ionospheric and atmospheric refraction effects to be determined separately. However, these and most of the other measurements that have been reported were conducted at latitudes and in directions for which the ionosphere would not be severely disturbed. Millstone Hill is ideally located for viewing both disturbed and more normal ionospheric conditions depending upon whether one looks north or south. Satellite passes to the north require vehicles with highly inclined orbits and the Navy Transit satellites as well as the NASA OGO series fulfill this requirement. These satellites carry beacon transmitters operating in the UHF band which opens the possibility of simultaneous angle-of-arrival measurements at the beacon frequency (~ 400 MHz) and the radar frequency (~1295 MHz). Further the orbits of the Transit satellites are known with sufficient accuracy to permit their positions to be used as checks on the accuracy of the refraction measurements and trajectory predictions made using perturbed data.

The program of work described in this document will be accomplished roughly in two main phases as indicated in Figure 2-1. Phase I, approximately 9 months in length, will be given to the instrumentation of Millstone for a dual frequency UHF-passive/L-band-active measurements program and to the study of data taken by other existing sensors. Phase II, occupying the remainder of a two-year period, will be concerned with obtaining new measurments at Millstone, together with analysis and reporting of the results. Auroral model studies and other theoretical work will continue throughout the program, as will consultation with BTL on system implications. In the remainder of this section we outline in broad terms the work to be carried out in the two phases. Sections 5 and 6 discuss in some detail the planned execution of the various tasks.

B. Phase I

i) Modifications to the Tracking Radar

The most significant change to the Millstone radar that must be accomplished during Phase I is the addition of the UHF passive lobe-comparison tracking feed and receiver arrangement to permit the arrival angle of signals transmitted by Transit and other suitable satellites to be determined. The antenna modifications and additions required for the passive UHF tracking system can best be described with reference to Figures 2-2 and 2-3. Figure 2-2 shows the tip of the tripod support for the Cassegrainian subreflector for the Millstone L-band radar. Above the subreflector is a hemispherical dome some 8 feet high which provides a controlled environment for receiver preamplifiers associated with radio astronomy feeds normally located at the prime focus of the 84-foot reflector. To permit the use of prime focus feeds, means are provided for removing the subreflector.

The proposed rearrangement is shown in Figure 2-3. An array of four crossed dipoles will be placed at the prime focus (behind the subreflector) in the location normally used for radio astronomy feeds. These dipoles are coupled together by means of a hybrid combiner which provides as output a sum channel and elevation and azimuth difference channels for both

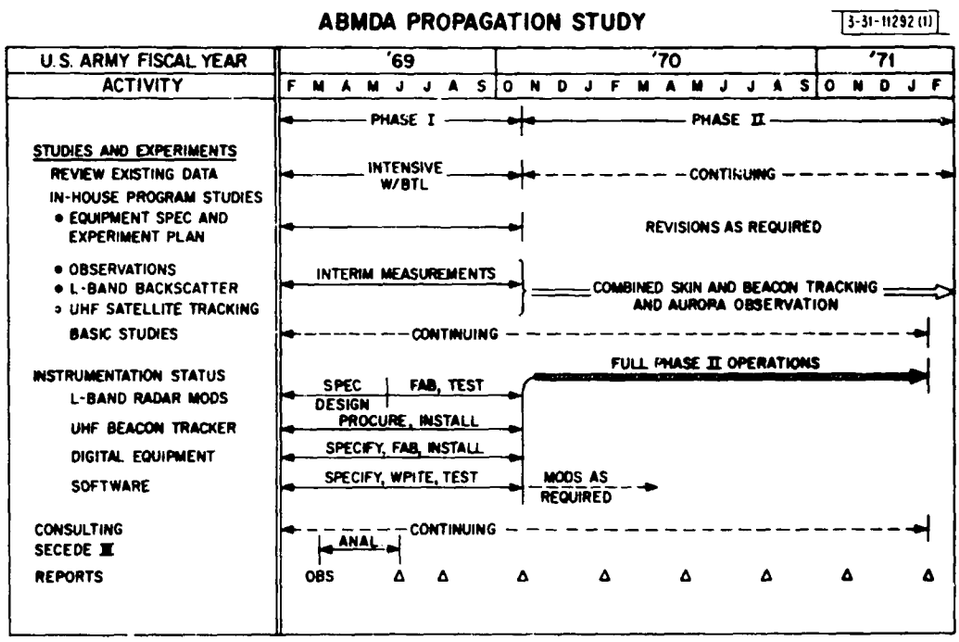

Fig. 2-1. Schedule of work for Millstone Hill Propagation Study Program.

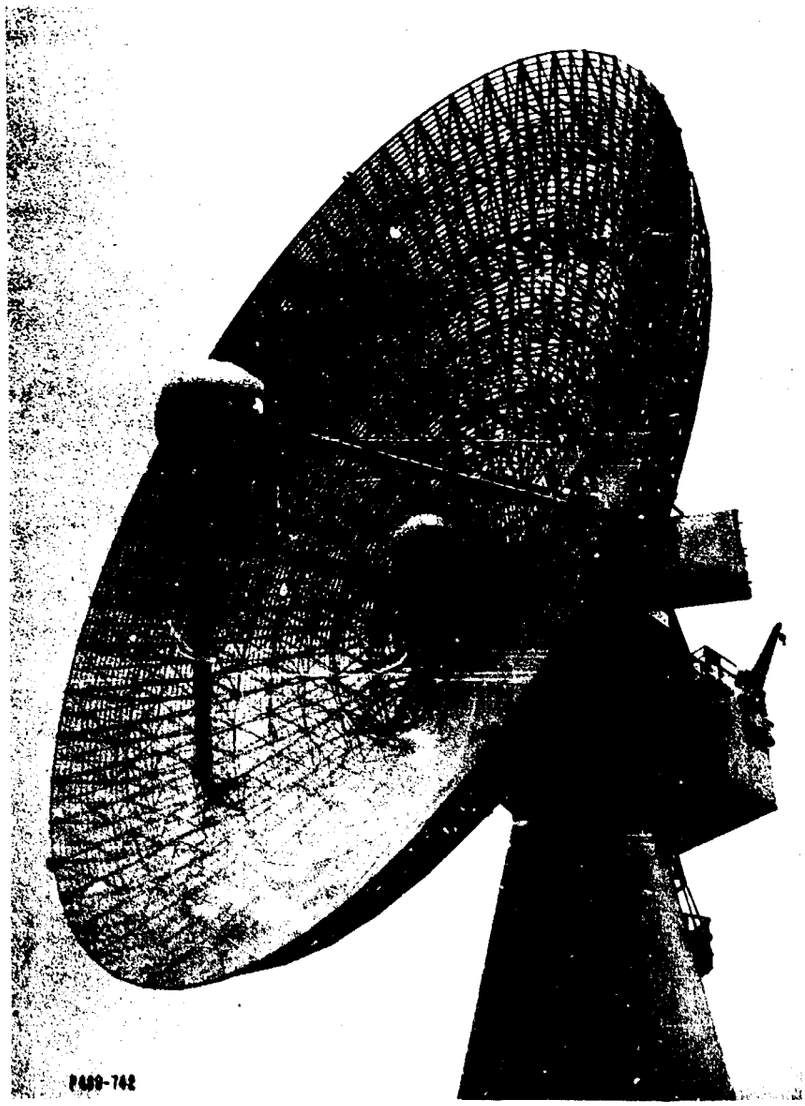

Fig. 2-2. Top of tripod subreflector support assembly of Millstone Hill radar antenna.

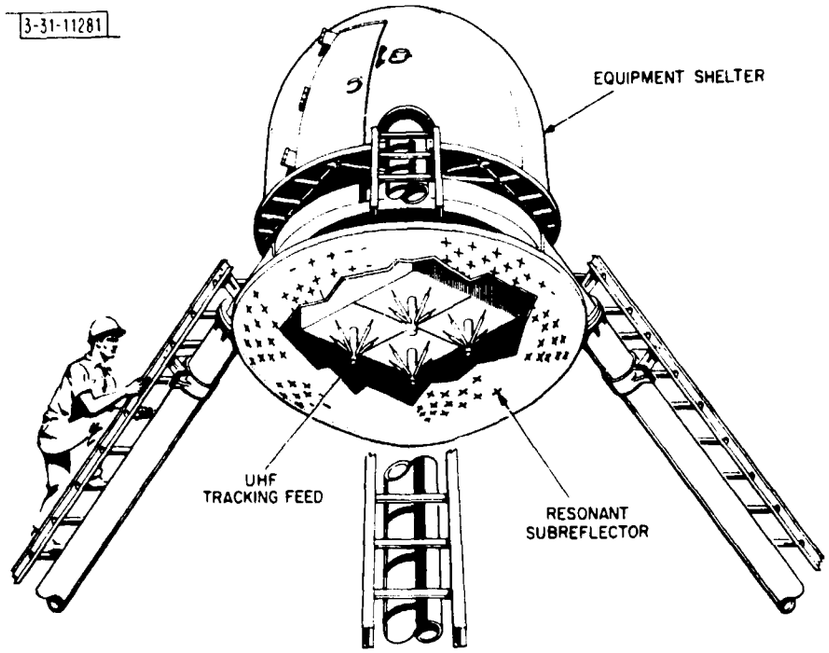

Fig. 2-3. New subreflector assembly for simultaneous L-band radar and passive UHF tracking operations.

polarizations (i.e, right and left circular). The associated UHF tracking receiver preamplifiers and mixers will be located in the environmental enclosure above.

In addition, since it is desired to provide for simultaneous use of the L-band radar, the present solid-skin subreflector is being replaced with a unit of molded dielectric faced with a mosaic of crossed dipoles, resonant at L-band. This reflector will permit signals received at UHF to be collected at the prime focus while reflecting the L-band energy for the Cassegrainian radar configuration. Virtually unimpaired radar operation should result and the effective aperture at UHF should be quite sufficient for the proposed application.

The completed system should be capable of

(1) Precisely tracking by radar any satellite within range (i.e., 8500 km for 1 meter^2 cross section).

(2) Passively tracking various satellites that have radio beacons operating in the vicinity of 400 MHz.

(3) Providing radar range, doppler, azimuth and elevation to the site computer.

(4) Providing both UHF and L-band monopulse boresight angle deviations, via appropriate analog-to-digital conversion equipment, to the Millstone computer for formatting and recording on magnetic tape.

(5) Providing similarly both UHF and L-band satellite signal amplitude data to the computer for formatting and recording along with other data. (Back-up chart recordings will also be provided for 'quick-look' and check purposes.)

(6) Recording L-band auroral backscatter data,namely range distribution and frequency spectrum,on magnetic tape for later analysis. This capability will obtain whether or not the radar is tracking a satellite target, in order that auroral conditions existing during a track may be evaluated.

(7) Driving the antenna under computer control in modes which:

(a) permit the gathering of satellite data with the antenna on program track (i.e., not auto-track);

(b) permit sector and elevation scanning appropriate to auroral backscatter studies.

These measurements capabilities are summarized in Table 2-1 and the overall interconnection of the various components in the system is depicted in Figure 2-4.

ii) Extension of Earlier Auroral Studies

During the current period when the UHF beacon tracking capability is being added to the radar a modest measurements and evaluation effort with the present L-band tracker is being pursued, and refinements of the experimental plan for Phase II are being worked out. This effort includes a continuation of existing studies on the radio aurora observed with the L-band radar (Abel and Newell 1969) with the following objectives:

(1) to obtain new estimates of the spatial distribution of auroral echoes and of the time variations of this distribution. Both long and short pulses are being used.

(2) to obtain the frequency power spectra of these echoes as a function of position within the auroral zone, and typical variations in the spectra with time.

(3) to search for and characterize so-called "discrete echoes" and to assess their potential as false targets.

(4) to conduct preliminary tests in which satellites are tracked through typical auroral disturbances. Such results would prove particularly interesting if appreciable scintillations are observed.

(5) to test several physical models for the occurrence and nature of the radio aurora against the new observations obtained.

Table 2-1

SUMMARY OF MEASURED PARAMETERS

L-Band Monopulse System

Satellite Skin Tracking

- Target Amplitude
- Range
- Range Rate
- Azimuth Boresight Error
- Elevation Boresight Error
- Azimuth
- Elevation

Auroral Backscatter

- Amplitude } as a function of range
- Spectrum } as a function of range
- Azimuth
- Elevation

UHF Beacon Tracking System

- Amplitude
- Azimuth Boresight Error
- Elevation Boresight Error
- Doppler

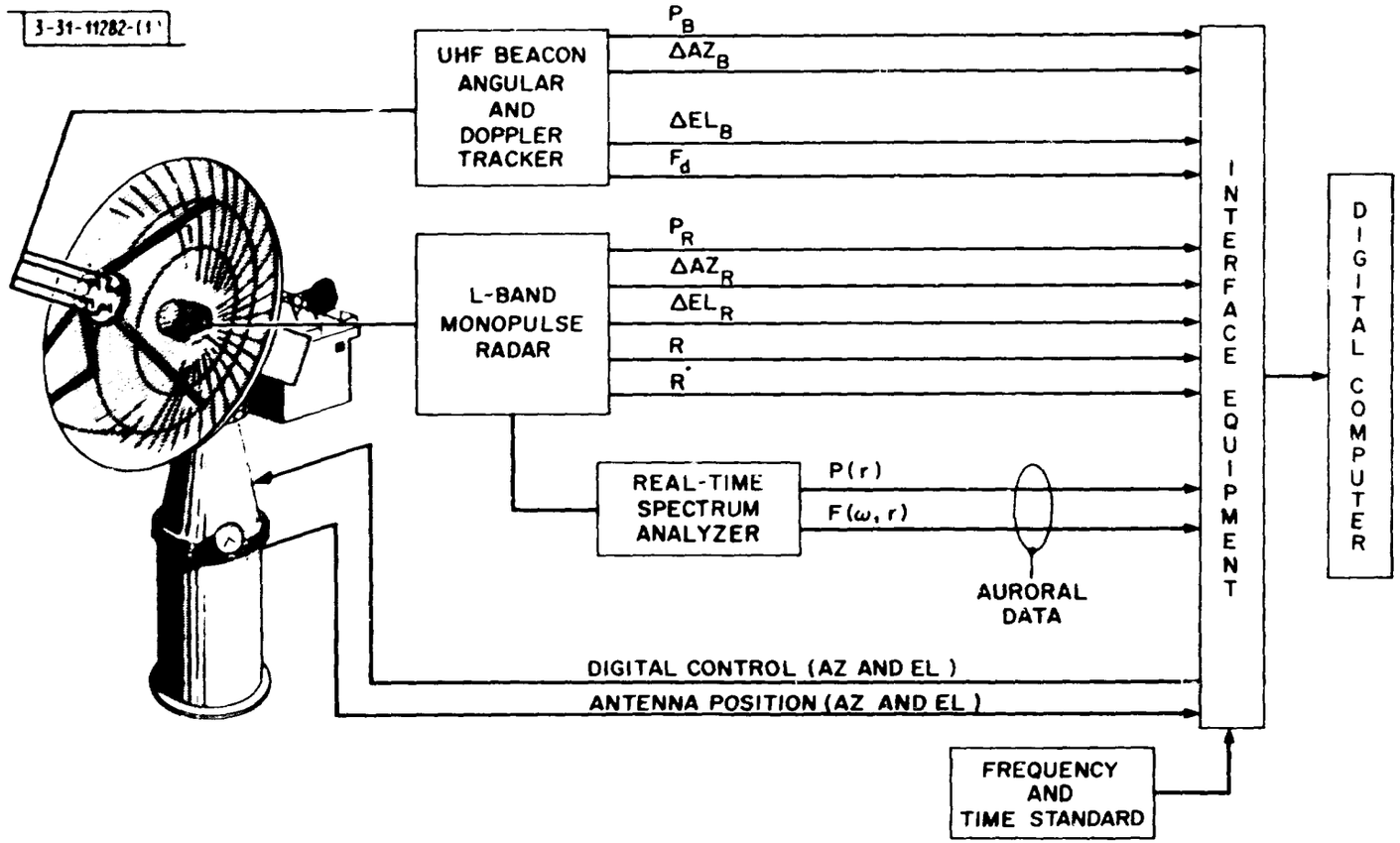

Fig. 2-4. Block diagram showing measurements capability of dual-frequency tracking system.

Implementation of this auroral study program is discussed further in Section 6.

Concurrent with this activity the possible utility of obtaining data from other sensors is being investigated. For example, arrangements have been made under which data on auroral echoes obtained by the Air Defense Command radar at Fortuna, N. Dakota will be collected and analyzed by Lincoln and BTL personnel (Section 6 C).

C. Phase II

This phase will begin when the overall instrumentation and programming task at Millstone is complete (Figure 2-1). It is anticipated that results of substantial interest will be forthcoming over a period of perhaps 16 months, making a total performance period for the program of 2 years.

During Phase II emphasis will shift to the collection of the types of data for which the revised Millstone system has been designed, i.e., coordinated measurements of angle-of-arrival at two frequencies, clutter from the intervening auroral zone and amplitude and phase scintillations. These measurements depend upon existing satellites such as the Transit and [illegible] family, which have appropriate UHF beacons. From these coordinated observations it is hoped to evaluate the measurement perturbations that may be encountered with the other radar systems and to separate the ionospheric from the tropospheric components. The innospheric perturbations should be an order of magnitude less at L-band than in the UHF channels, while the tropospheric component should be of the same order (Section 3). It follows that the use of a single antenna system for simultaneous measurements makes less important the estimation of atmospheric refraction, since the differential in the electrical measurements of the two off-boresight angles is directly related to the ionospheric component of the angular scintillations. Nonetheless (as discussed in Section 5 A) care will be used in monitoring and updating the absolute pointing errors of the antenna to permit the total refraction of the beam to be estimated to an accuracy of about 0.02 degree so that data on tropospheric refraction can be obtained also. In order to

achieve this absolute precision the capabilities of an anti-backlash feature of the antenna drive, which was added in 1965-6, will be exploited.

There exists the possibility that refraction and angular scintillation data may be compromised by multipath effects due to ground reflections. Although it is not possible to determine precisely in advance the magnitude of this effect, a rough estimate, based upon existing data (Section 5 D) suggests that these effects should be completely negligible to above about 2° elevation.

The intensity of both the UHF beacon signals and the L band echoes will be recorded to show the effects on the signal of propagation (particularly through aurora) as a function of time. Amplitude scintillations are important since they limit target detectability and accuracy of tracking, and because they compromise simple first-order attempts at target discrimination.

The extent to which amplitude and angle scintillations are correlated and their relationship to auroral backscatter and visual auroral forms has yet to be established. The experimental system provides for the recording of auroral backscatter simultaneously with tracking operations in order to provide data in this area. In addition, on days when favorable satellite tracks are available, it is planned to obtain radar coverage as completely as possible of the aurora near the times of the track.

As an adjunct to the continuing use of the Millstone Radar for the two-frequency studies, an average of one operating day per week will be devoted to the gathering of auroral backscatter data for continued basic studies of the phenomena involved. In this work tests of specific hypotheses will be emphasized rather than routine gathering of synoptic data. It may also be that Thomson scatter measurements (Evans 1969) with 220-foot UHF zenith-looking radar will be valuable in more completely understanding the ionospheric situation on auroral days.

It is planned to attempt to obtain corroborative records of magnetic and optical activity in the auroral zone, as well as satellite and aircraft soundings of conditions related to the auroral events observed at Millstone, whether or not these are in connection with satellite tracking operations. In addition, as discussed in Section 5 F, there are plans to obtain data on the spectrum and intensity of particles precipitating in the auroral zone using instruments mounted on a Lockheed satellite that is already in orbit.

3. Review of Atmospheric and Ionospheric Refraction

A. Introduction

In this section we briefly review the phenomenon of atmospheric and ionospheric refraction including scintillation effects. A number of authors have discussed these effects in great detail and the reader is referred to Millman (1961) for a general review. Atmospheric effects on radio propagation are reviewed at length by Bean and Dutton (1966) while ionospheric effects at VHF and UHF have been described by Lawrence et al. (1964) and Voronin (1964). The material presented here has been taken largely from a review by Rogers and Evans (1968).

B. The Lower Atmosphere

For convenience in study and description, the earth's lower atmosphere is usually divided into two regions: the troposphere and the stratosphere. The troposphere extends from the earth's surface up to an altitude of, very roughly, 10 kilometers, but it may vary from as low as 7 km at high latitudes to as high as 18 km at the equator. Throughout the troposphere the mean temperature decreases approximately linearly with the altitude, from a surface value near 290°K to one of about 220°K at the tropopause. Above the tropopause, i.e., the upper altitude limit of the linear temperature profile, the mean temperature tends to remain more or less invariant with altitude up to about 30 km -- thus giving the name stratosphere to this latter region. Subsequently the temperature increases with height, and continues to do so up to about 50 km where it reaches a maximum called the stratopause.

Throughout the troposphere and stratosphere the mean absolute pressure, P, decreases approximately exponentially with height; it has decreased to about one-quarter of its ground level value at the tropopause. The average water vapor content, ρ, also falls very rapidly from that at ground level, becoming very small above the troposphere.

Good approximations to these exponential decays are given by:

$$\frac{P}{P_o} = \exp(-h/a) \tag{3-1}$$

where

$$a \cong 7 \text{ km}$$

and

$$\frac{\rho}{\rho_o} = \exp(-h/b) \tag{3-2}$$

where

$$b \cong 2 \text{ km}$$

and where h is the height in km.

The relative concentrations of the major neutral gas constituents except for uncondensed H_2O vapor -- remain essentially constant up to an altitude of about 20 km. Immediately above this general region, the relative concentration of molecular oxygen begins to decrease somewhat, and O_3 (ozone) appears.

It will be appreciated that the foregoing statements are, of necessity, qualitative in nature. There are variations in absolute pressure, partial H_2O vapor pressure and temperature with time location and altitude. Over short distance and time scales such variations can be large and intense. Also, much of the lower atmosphere often contains cloud and fog droplets, rain drops, snow and hail. The occurrence, concentration and extent of these latter atmospheric constituents can usually only be described in very approximate and/or statistical terms. All of these variations influence radio wave propagation in the earth's lower atmosphere -- sometimes in an abrupt and marked manner.

C. Refraction in the Lower Atmosphere

The refractivity exhibited by the neutral gases which predominate in the earth's lower atmosphere is related to the physical characteristics of the gaseous mixture as follows.

$$N = (n - 1)10^6 = 77.6 \frac{P}{T} + 3.73 \times 10^5 \frac{e}{T} \qquad (3\text{-}3)$$

where

N = refractivity

n = refractive index

P = absolute atmospheric pressure, in millibars

e = water vapor pressure, in millibars

T = absolute temperature in degrees Kelvin

The refractive index near the earth's surface departs from the value of unity (for a vacuum) by some 300-400 parts/million and is essentially independent of frequency throughout the cm-mm wavelength region. Equation (3-3) indicates the predominant effect of uncondensed water vapor upon the refractivity of the earth's lower atmosphere. Since the average water vapor concentration decreases rapidly (approximately exponentially) with height, so does the refractivity. The value of N approaches unity in the lower regions of the stratosphere. In addition, the water vapor concentration, both absolute and as a function of altitude, changes markedly with time and therefore the refractivity does also. These refractivity variations are capable of exerting a great influence on the propagation of radiowaves in the troposphere, especially at lower altitudes and for near-horizontal ray paths. Studies of this influence are often subdivided into the steady-state influences associated with the mean value of refractivity, and the influences of variations from the mean.

The fact that there is a nearly exponential decrease of average refractivity with height requires that exact measurements of distance, velocity or angular position by means of radio waves must be appropriately

corrected in order to yield the correct absolute values. For instance, for a measurement of range to a far distant object($\gtrsim$ 500 miles, approximately) made at an elevation angle of zero degrees and a surface refractivity of ~350, a correction of some 350 feet would have to be made. For an extreme value of the surface refractive index i.e., some 450 parts/10^6, this correction would increase to nearly 600 feet; at a measurement elevation angle of 3° it would reduce to some 100 feet.

Under the same circumstances of surface refractivity and elevation angle, the first order correction to be applied for the elevation angle error would be respectively ~17 milliradians, ~32 milliradians and ~5 milliradians. From these examples it can be seen that only extremely accurate distance measurements would need a refractivity correction, but that elevation angle corrections may be required.

The surface value of the refractive index and its rate of change with height vary with geographical location, with season and often over the day-night cycle. Complex variations in the slope and even sharp layers in the refractive index profile can be observed in some locations and/or seasons as much as one-half of the time. This results in a usually relatively slow, but continuous, variation in the radio wave path length and a wander in the angle of arrival. For instance, the wintertime standard deviation about the mean correction to be applied to an elevation arrival angle of 1° is some 0.3 milliradian, with a value of ~1 milliradian being exceeded 1% of the time. Although these fluctuations were measured in elevation, comparable fluctuations in azimuth seem likely. As a c[illegible]ence, the most exact radio wave measurements of angle require correction for the atmospheric refractive index conditions existing during the measurement interval. The simple use of the surface value of the refractive index and its implied mean profile slope is of assistance in this regard, but local measurements with radiosonde or airborne microwave refractometer instruments, especially when combined with ray-tracing techniques, are necessary for determining the corrections with the greatest accuracy. (See for example Hughes et al. 1964)

Superimposed upon these relatively slowly varying components of the refractive index is a continuous variation in the small-scale spatial and temporal value caused by irregular inhomogeneities in the lower atmosphere. This causes, in turn, a short-time scintillation in an electrical path length and ray angle of arrival. Short time variations of 5 electrical degrees have been measured at 1000 MHz in the summertime along a path of ten miles slanted in elevation at the rather large angle of 9°. Two antennas separated by 500 feet along the same path have been employed to measure relative phase at a wavelength of 3 cm. Variations of as much as 40 electrical degrees were observed, with typical periods of 10-100 seconds. In another case, an angular scintillation of some 0.1 milliradian was observed at 3 cm with a periodicity of the order of about a second.

The implications are that in the limit, even after corrections for both the average and the slowly varying refractive index changes, there still remains a short-time scintillation component which could place a fundamental limit upon very accurate angle measurements and upon the full realization of the plane wave gain of very high-gain antennas. It would appear that, even for substantially elevated angles, difficulties will be encountered at some mid-latitude locations in the Northern Hemisphere in measuring angular accuracies to better than a few tenths of a milliradian. Hence plane wave gains of fixed antennas greater than, roughly, 50-60 db might not be continually maintained when pointed at the horizon or 70-80 db even pointed well above the horizon. Again, concern with extreme angular measurement accuracy and/or antenna performance requires that attention be paid to local radio-climatological characteristics, and might limit operation to the higher elevation angles.

It is not as yet quantitatively clear to what extent clouds or solid particle concentrations along the radio path would worsen these refraction effects, although it appears that clouds may be important and the combination of short radio wavelength and high intensity rainfall can also apparently result in serious perturbations of a nominally plane wavefront.

For propagation elevation angles $\leq 10^{\circ}$ approximately, fading can be expected at least as a result of air-to-air multipath, and, for sufficiently wide vertical antenna radiation patterns, as a result of interference between direct and surface-reflected rays. The occurrence and depth of this fading increases rapidly with decreasing angle below 5°.

Finally, it should be noted that variations in the gradient of the refractive index slope and the presence of elevated layers and turbulent irregularities permit short radio waves to propagate very far beyond the normal radio horizon.

D. The Ionosphere

i) General

Above an altitude of ~60 km the atmosphere is ionized by solar ultra-violet radiation. This ionization is removed by a number of competing processes so that at no altitude is the air completely ionized though the fraction increases with height reaching ~1% at 300 km. Typical profiles of electron density vs. altitude are shown in Figure 3-1. These profiles vary with time of day, season, sunspot cycle, latitude, longitude and magnetic disturbance activity. This variability makes it extremely difficult to define acceptable models for the electron density from which useful predictions of ionospheric refraction can be obtained. A further difficulty is that there is no simple equivalent of a radiosonde that can provide the refractive index throughout the layer. This can be determined using high altitude rockets or Thomson scatter soundings but these methods are complex and expensive. The swept frequency H.F. radar (ionosonde) that explores the virtual height of the reflecting layers can yield information only up to the peak of the F2 layer (Figure 3-1). This is inadequate to define the refractive index at all altitudes, but does go some way toward a solution because i)the refraction at any point is proportional to the rate of change of density along the ray path and the steepest gradients are always on the bottom side and ii)the zenith distance to the ray increases with altitude (due simply to earth curvature)thereby making the path less oblique.

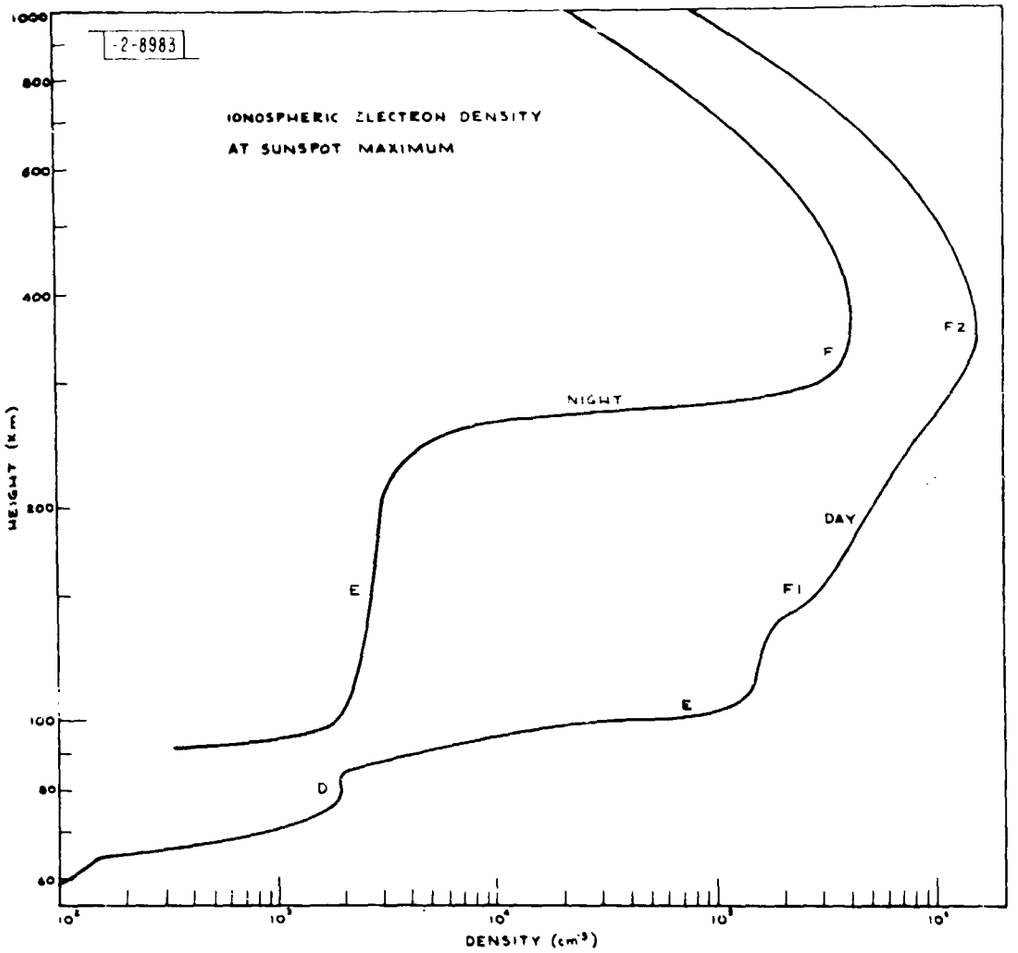

Fig. 3-1. Idealized electron density distribution in earth's ionosphere. Curves indicate densities to be expected at sunspot maximum in temperature latitudes.

In the absence of any other sources of information useful predictions of the electron density distribution can be obtained by adopting a model for the layer shape and normalizing the peak density to match the critical frequency given for the date, time, latitude and longitude in the Institute for Telecommunication Sciences (Environmental Science Service Administration) bulletin of Ionospheric Predictions. These, however, become extemely inaccurate over polar regions where there is an inadequate number of ionosonde stations. Models of the ionosphere such as these assume the existence of smooth spherically stratified layers. While this may be accurate in certain places for part of the time, it is never wholly correct. Irregular structure of various scales are frequently present. Three which may be recognized readily from conventional ionospheric sounding are sporadic E, spread F, and Travelling Ionospheric Disturbances (T.I.Ds), and are discussed below.

ii) Sporadic E (Es)

A typical daytime ionogram normally would exhibit a critical frequency of about 3 MHz for the E trace. At other times, however, the E region echo observed on an ionospheric sounder will extend over many megahertz. The layer which gives rise to this echo must be thin because the height of the echo (Es) appears to be independent of frequency and the F region can be seen through it. The appearance of this echo is not always the same and attempts to classify it into different types do not appear to have helped greatly in understanding the phenomenon. The occurrence of Es for three different latitudes is shown in Figure 3-2. It seem possible that many independent causes may give rise to this phenomenon. For example in auroral regions the auroral ionization itself may be responsible while over the equator large scale density irregularities associated with a current system known as the electrojet are the agent. At temperate latitudes it seems that wind shears can cause long-lived metallic ions produced by ionization of meteoric debris to be driven into thin layers.

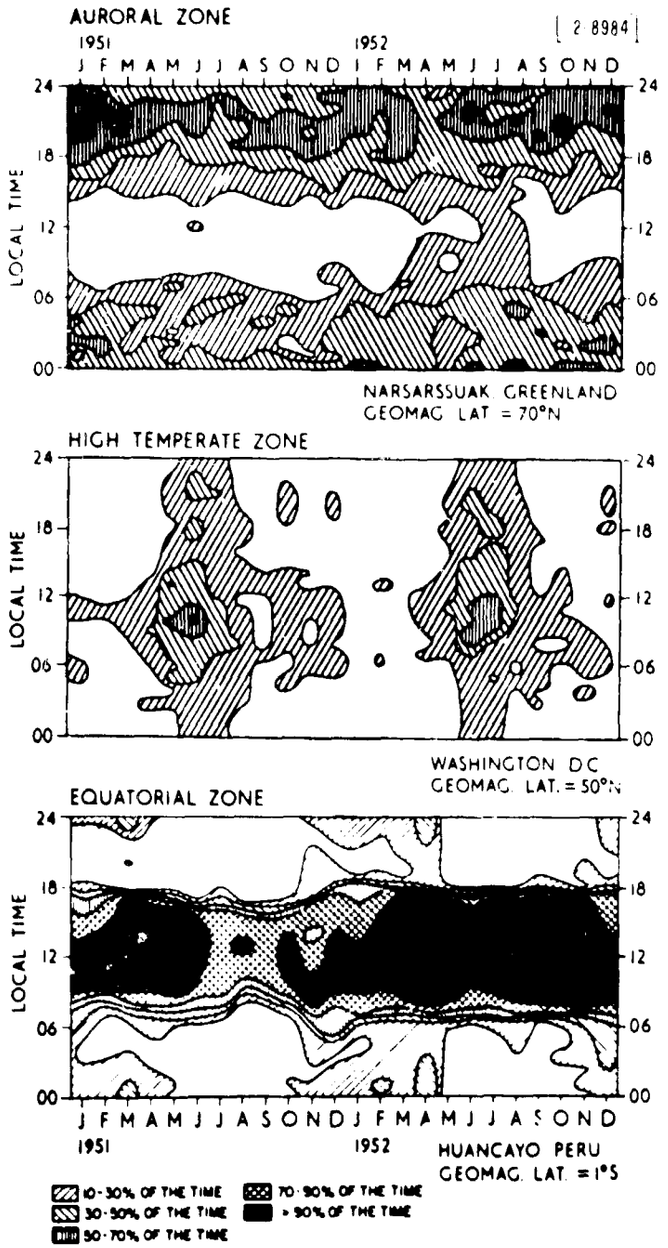

Fig. 3-2. Occurrence of sporadic E echoes (E_s) for three stations at different latitudes according to E. K. Smith, 1957.

iii) Spread F

Frequently the F region echo observed with an ionosonde takes the form of an irregular band of reflections. The condition is called spread F, as it appears that the reflected pulse is elongated by the presence of scattering regions at different ranges. It is not clear whether the different scattering regions are arranged at different vertical distances from the transmitter or if they are at different horizontal distances from the point immediately above the transmitter.

The occurrence of spread F -- chiefly at night -- is well correlated with the occurrence of scintillations of radio stars. By means of the topside sounder Alouette it has been possible to map the geographic location of Spread F (Figure 3-3). Principal regions are located in the auroral zones and over the geomagnetic equator at night. No one theory has been put forward which explains all the observations relating to spread F.

iv) Travelling Ionospheric Disturbances

Very large scale irregularities have been shown to be present quite frequently in the F region. These irregularities have been studied extensively by means of reflected signals, and have been given the name Travelling Ionospheric Disturbance (TID). They may be recognized on fast run ionosonde records as vertically traveling cusps. The disturbances have a scale size of ~ 200-400 km and travel (horizontally) with a speed of ~ 100 m/s, chiefly from north to south. For reflected signals they cause the angle of arrival to fluctuate by ~ $\pm 2^{\circ}$. Evidence for the presence of these same disturbances has also been obtained from observations of radar signals reflected from the moon and of signals received from satellites. It appears that they cause the number of electrons integrated along the ray path to fluctuate by ~ $\pm$ 2%. Using Thomson scatter soundings it has been found that the waves appear as compressions and rarefactions as well as a corrugation of the layer. Below about 250 km the progression of phase is downward with time. Upward through the F region maximum, however, the phase fronts are found to slope toward the vertical. Such structure is believed to be caused by motions in the neutral atmosphere called internal atmospheric gravity waves.

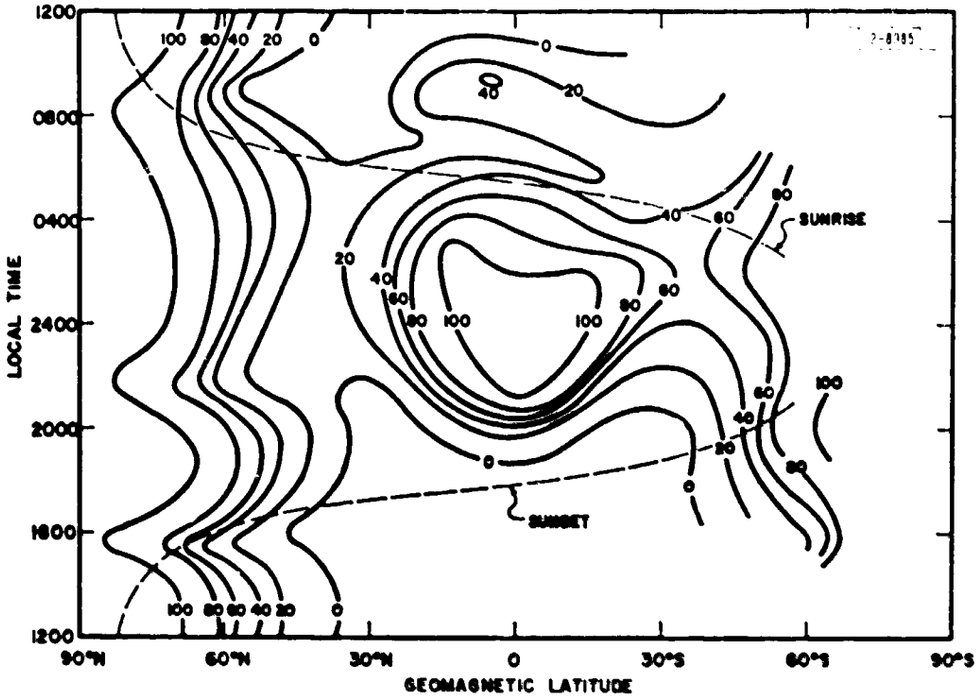

Fig. 3-3. The percentage occurrence of spread F. (After Calvert and Schmid, 1964.)

E. Refraction by the Whole Ionosphere

Atmospheric refraction of radio waves (discussed in part C of this section) will occur for all radio waves irrespective of frequency. Ionospheric refraction on the other hand is frequency dependent, and arises only because of the curvature of the ionosphere. If the ionosphere were indeed a plane slab of uniform thickness suspended above a plane earth, a ray would emerge at the same angle as the angle of incidence -- since the refractive index on either side of the slab is close to unity.

The total bending R of a ray r out to a point at a height h will be

$$R = - \int_0^h \frac{\tan \theta}{n} \cdot \frac{dn}{dr} \cdot dr \qquad \text{radian} \qquad (3\text{-}4)$$

where θ is the local angle of incidence of the ray at r and n the local refractive index. In the ionosphere $n \leq 1$ but since the sharpest gradients dn/dr occur on the bottomside and $\theta \to 0^\circ$ with increasing altitude the downward bending of the ray in the lower ionosphere is not offset by an equal upward bending on the topside (i.e., above h_{max} F_2). Thus the effects of ionospheric refraction are to increase the angle of arrival of radio waves above the true angle of the altitude of the source, i.e., the effect has the same sense as atmospheric refraction. For VHF and UHF the refractive index is given in

$$n^2 = 1 - \frac{N_e e^2}{\pi m f^2} \qquad (3\text{-}5)$$

where f is the radiowave frequency, N_e the number, e the charge, and m the mass of the electrons. Computing ionospheric refraction therefore reduces to making a model for N_e as a function of distance along the ray path. Usually spherical symmetry is assumed and then the electron density may be expressed only as a function of height.

Curves showing the refraction to be expected at different frequencies are given in the "Handbook of Geophysics" (1960). These were computed by using a model for the ionosphere which consists of three rectangular slabs representing the E, F1 and F2 regions. It seems probable that this gross simplification leads to considerable error in predicting the refraction. Somewhat more realistic models have been employed which assume that the refraction is principally caused by the F2 region and that this has a parabolic electron density distribution. For this type of layer the total bending R becomes

$$R = \frac{2d}{3a} (f_c/f)^2(1 + h_m/r_o) (\sin^2\theta + 2h_m/r_o)^{-3/2} \cos \theta \qquad \text{radian} \quad (3\text{-}6)$$

where d = the semithickness of the parabolic layer, r_o = radius of the earth, f_c is the critical frequency of the layer, f the radio wave frequency, h_m = height of maximum electron density and θ is the apparent altitude of the radio source. Where the upper and lower parts of the F region may be represented by different parabolas having semithickness of d' and d (respectively), the term 2d (in Equation 3-6) must be replaced by $(d + d')$.

If a more realistic shape than two parabolic sections is chosen to represent the ionosphere, then analytic solutions become unpractically complex and a ray tracing procedure must be adopted. Weisbrod and Anderson (1960) have shown, however, that there is an approximate procedure which can be employed with any given electron density profile.

Though the principal effect of ionospheric refraction is to change the apparent altitude of a source, small changes in the apparent azimuth are also possible. There are believed to be caused by a prism or wedge-like distribution of electrons which can be formed near sunrise or sunset.

F. Effects of Large-Scale Irregularities

Traveling Ionospheric Disturbances (TID) are observed to have quasi-wavelengths in the range 50 to 400 km and to have speeds of up to 350 m/s. The direction of the drift motion is principally towards the south. For reflected signals the rms tilt of the reflecting surface from the mean spherical surface is of the order of $\pm 2^{\circ}$. The existence of this phenomenon means that the gross refraction introduced by the ionosphere (discussed previously) is subject to random irregular changes introduced by wavelike structure within the ionosphere. It is not difficult to estimate the extent of this effect. The local tilting will cause the angle at which the rays strike the ionosphere to change by $\pm 2^{\circ}$. This is approximately what would happen if the ionosphere did not change but the true bearing of the source changed by $\pm 2^{\circ}$. The amount of refraction might then be expected to fluctuate by $\approx \pm 10\%$ in the worst case -- when the zenith distance approaches 90°.

As an example, scintillations of the apparent position of the radio source in Cygnus A observed by means of an interferometer at 108 Mc/s have been reported. At elevations below 20° random deviations as large as $\pm 0.5^{\circ}$ have been observed which were attributed to TIDs. Similar effects have also been reported based upon observing geostationary satellites at low altitudes (Elkins et al 1968). These authors found that for a station near Boston and observations toward the south ionospheric effects dominated at VHF (136 MHz) but at UHF (408 MHz) atmospheric effects were the more important.

G. Effects of Small-Scale Irregularities

i) Observations

A more damaging form of irregular refraction is that associated with the spread F condition in the ionosphere. The presence of small-scale irregularities within the ionosphere introduces random phase changes in the wave front of a plane wave which traverses it. As a result the phase of the wave will not be constant over the ground but will form an irregular pattern. This pattern will in general appear to move as a consequence of (a) the

motion of the target behind the diffracting screen, and (b) the existence of winds in the ionosphere which cause the irregularities to move principally towards the east or the west. The result is that the position, phase and possibly also the intensity from a distant source will appear to fluctuate.

The effect is well correlated with the occurrence of Spread F and hence is chiefly a nighttime phenomenon. Figure 3-3 shows the percentage occurrence of spread F over the globe inferred by Calvert and Schmid (1964) from topside soundings. It can be seen that the phenomenon is intense over the geomagnetic equator at night and present in the auroral regions both by day and night. It is least likely to be observed at midlatitudes.

The horizontal dimensions of the irregularities appear to be of the order of a few km and it is also believed that they are considerably elongated along the lines of the magnetic field. The apparent wind speeds lie in the range 50-300 m/s.

ii) Phase Scintillations

In addition to the experimental work (which in recent years has included observations of artificial earth satellite signals) there has been a large measure of theoretical interest in the problem of radio waves traversing a phase changing screen. The theory has been summarized by Lawrence et al. (1964) who show that if irregularities are of effective length L in which the electron density departs from its median value N_e by an amount dN_e then the mean square phase deviation introduced by a single irregularity will be

$$\left(\frac{2\pi L}{\lambda}\right)^2 \overline{\left(\frac{dn}{n}\right)^2} \qquad (3\text{-}7)$$

where n is the refractive index (Eq. 3-5). In a distance D along the radio path, there will be ~ D/L irregularities if they all have the same size. Thus

the total mean square phase deviation will be

$$\overline{(\Delta\phi)^2} = \frac{D}{L} \left(\frac{2\pi L}{\lambda}\right)^2 \overline{\left(\frac{dn}{n}\right)^2} \tag{3-8}$$

which in terms of electron density fluctuations becomes

$$\overline{(\Delta\phi)^2} = \frac{D}{L} \left(\frac{2\pi L}{\lambda}\right)^2 \frac{f_c^{\,4}}{4f^4} \overline{\left(\frac{dN_e}{N_e}\right)^2} \tag{3-9}$$

and may be expressed as

$$\overline{(\Delta\phi)^2} = \frac{\pi^2}{c^4} \, DL \, f_c^{\,4} \lambda^2 \overline{\left(\frac{dN_e}{N_e}\right)^2} \tag{3-10}$$

where c is the velocity of light, and f_c the critical frequency $[=(N_e e^2/\pi m)^{\frac{1}{2}}]$. Thus the rms phase fluctuations are proportional to the electron density N_e and the radio wavelength λ (or inversely proportional to the frequency f).

From Equation (3-10) we see that $\overline{(\Delta\phi)^2}$ depends upon the product of D and L and if it be assumed that L is independent of zenith angle i (i.e., the irregularities are spherical in shape) it would be expected that

$$\overline{(\Delta\phi)^2} \propto \sec i \tag{3-11}$$

where i is the local zenith angle at the ionosphere

$i = \sin^{-1}\{r_o \sin \chi_o/(r_o + h)\}$ where r_o = earth's radius

h = height of irregular diffracting layer and χ_o = zenith angle at the observer.

Departures from this law have led to the conclusion that the irregularities are not circularly symmetrical but elongated along the geomagnetic field lines with a ratio of major to minor axes of at least 5:1.

There are few reported measurements of the phase stability of transmitters beyond the earth's ionosphere, though many measurements of amplitude effects (next section) have been reported. One method which promises good results is the phase coherent examination of stable satellite signals. The large Doppler shifts introduced by the motion of the satellite must be removed by a least mean square quadratic fit to the record so that the residuals may be determined. In this way rms phase fluctuations of the order of 2 radians at a frequency of 324 Mc/s have been observed.

iii) Amplitude Scintillations

Although intensity fluctuations of radio stars or artificial earth satellites have been the primary means of observing small scale ionospheric irregularities, this is by no means the best method, as in general the phase or angular scintillation effects are more pronounced. For there to be pronounced amplitude scintillations, it is necessary that angular refraction for two or more rays to be large enough that they can interfere at the ground. The relevant theory shows that this in turn depends upon the distance of the observer from the diffracting screen. An irregularity of scale L subtends one Fresnel zone when viewed at a distance z_f where

$$z_f = \frac{(2\pi L)}{\lambda} \qquad (3\text{-}12)$$

If the scatters are located physically closer than this at a distance z then the mean square fractional deviation in amplitude $[\overline{(\Delta A)/A}]^2$ is related to the mean square deviation in phase $\overline{(\Delta\phi)^2}$ by

$$\overline{\left(\frac{\Delta A}{A}\right)^2} = \left(\frac{z}{z_f}\right)^2 \overline{(\Delta\phi)^2} \qquad (3\text{-}13)$$

For ionospheric irregularities z_f is usually of the order of several thousand km and the ratio $(z/z_f)^2$ may be as small as 1/25. Thus if the rms phase fluctuation is of the order of one radian or less the amplitude fluctuations will be unimportant. In view of the above remarks it is clear that the values of the amplitude fluctuations reported in radio star scintillations can only be converted to provide a measure of the more important phase or angular fluctuations if the size and height of the irregularities are known.

The zenith angle dependence of amplitude scintillations, has been studied by a number of authors. An amplitude scintillation index S may be defined which is related to the signal intensity R in

$$S^2 = \frac{\overline{R^4} - \overline{(R^2)^2}}{\overline{(R^2)^2}} \tag{3-14}$$

This index is related to the mean square phase fluctuation $\overline{(\Delta\phi)^2}$ in

$$S^2 = \overline{2(\Delta\phi)^2} \left(1 + \frac{\pi^2 L^4}{4\lambda^2 z^2}\right)^{-1} \tag{3-15}$$

where λ is the radio wavelength and z the distance to the irregularities. It then follows that the zenith dependence of amplitude scintillations is of the form

$$S^2 \propto \lambda^2 \sec i. \left(1 + \frac{\pi^2 L^4}{4\lambda^2 z^2}\right)^{-1} \tag{3-16}$$

where i is the zenith angle at the ionosphere.

iv) Angular Scintillation

Fluctuations in the angle-of-arrival of radio waves from a strong radio source have been observed by means of interferometer observations at temperate latitudes. At a frequency of 108 MHz the rms angle through which the source scintillates $\sqrt{\theta^2}$ is of the order of $.03^\circ$ and at 53 Mc/s it is $\sim 12^\circ$.

When observations are made by means of an interferometer, and the correlation between the phases of the signals received on the two antennas (separated by d) is ρ then the mean square angular fluctuation $\overline{\theta^2}$ is given in

$$\overline{\theta^2} = \frac{(1 - \rho)DLf_c^{\,4}}{2f^4} \overline{\left(\frac{dN_e}{N_e}\right)^2} \qquad (3\text{-}17)$$

Evidently $\sqrt{\theta^2}$ is proportional to $1/f^2$, and must depend upon sec χ_o (as the path length D increases with increasing zenith angle).

If the ionospheric irregularities lie chiefly in a layer which is thin compared to the total thickness of the F layer it becomes possible to present a simple theoretical description of the scattering phenomenon. Suppose that for different distances along the screen the phase shift $\Delta\phi$ introduced varies and this can be described by a horizontal correlation function $\rho(d)$, which is of the form

$$\rho(d) = \exp\left[-\tfrac{1}{2}(d/d_o)^2\right] \qquad (3\text{-}18)$$

If the distribution of values $\Delta\phi$ is also a gaussian function with an rms phase deviation Ω_o then the angular distribution of the diffracted rays will be

$$\sigma(\theta) = \exp\left[-\tfrac{1}{2}(\theta/\theta_o)^2\right] \qquad (3\text{-}19)$$

Two cases can be considered. Where the phase fluctuations are small, i.e., Ω_o is less than one radian $\theta_o = \lambda/2\pi d_o$. In this case the pattern of phase fluctuations on the ground matches that introduced in the ionosphere, and rays never cross so that amplitude fluctuations remain small. Where, however, $\Omega_o \gg 1$ radian then $\theta_o = \Omega_o/d_o$. In this case the angular scintillation is proportional to the ratio of the scale of the

phase deviation, to the horizontal correlation length in the screen.

In sum, when amplitude scintillations are detected angular and phase scintillations must also be present, though the reverse is not necessarily true.

4. Review of Radio Auroral Echo Phenomena

A. Introduction

Radio aurora is the name given to ionization irregularities in the auroral zone responsible for the observed reflection of radio waves. The term is also sometimes extended to include radio signals thought to be emitted from the auroral zone; the evidence for such signals, reviewed recently by Ellyett (1969), is relatively weak and it is difficult to distinguish emissions from reflections originating from distant radio transmitters.

Reflections from radio aurora have been observed and documented since the middle 1930's and much of the continuous and extensive survey work has been done by radio amateurs working in the 40-150 MHz region with relatively low power levels (about 100 watts), who found that by directing both transmitter and receiver northward towards the auroral zone, they could communicate much better than if their antennas were directed along a line of sight. There are a number of quite comprehensive reviews of radio auroral work and its interpretation, for example, Booker (1960), Chamberlain (1961), Bagaryalskii (1961), Hultqvist and Egeland (1964), and Lange-Hesse (1968), as well as extensive accounts of results by individual groups; for example, Leadabrand et al. (1965) and Chestnut et al (1968) have described the work by the Stanford Research Institute, Unwin and Knox (1968) and references therein dealt with the work in New Zealand.

Rather than reiterating this review material an attempt will be made to summarize the presently known facts about radio aurora without extensive citation, and from the perspective of current theories, which will also be outlined. In addition a brief survey of the information now available concerning the ingredients of the theories is included. The relationship between radio auroral and other geophysical parameters possibly pertinent to the propagation problem is discussed. Some of the questions relating theory and observation which present and future studies may help to answer are raised in Section 6 B.

B. Spatial Distribution and Time Dependence

In general, scattering is only observed from the auroral zone and is mostly from the E-region. Forward-, oblique- and back-scatter observations have been made. Scattering occurs from field aligned irregularities and is only appreciable in directions perpendicular to the magnetic field. The magnetic geometry of a particular site is thus of paramount importance and the aspect angle is a major factor in controlling echo distribution. (See Section 6 C).

From Millstone for example, there are two points at a height of 110 km where the perpendicularity conditions are met at a range of 1000 km, each about 20° in azimuth away from the magnetic meridian at 345°. The spatial distribution thus depends on the existence of scatters in the right position. The scatterers seem to be confined to the auroral zone or more precisely to the auroral electrojet current cores. Such cores, as a function of geomagnetic latitude and local time, are shown schematically in Figure 4-1 (after Sugiura and Heppner, 1965). The currents in this classical picture were deduced from ground-based magnetometer readings. The cores move southwards towards local midnight, reverse direction around local midnight, and are most intense in the evening and night quadrants. The so-called "afternoon echoes" measured at Millstone have a horizontal north-south range extent of, typically, several hundred kilometers and usually extend northwards beyond the radar horizon.

In the east-west direction there is a tendency for echoes to appear most strongly at the two favorable aspect angles, one on each side of the meridian, and the total extent, while often approaching 1000 km, is also limited by the magnetic geometry. The true echo dimensions are of course smeared by the beam-width pulse-length influence in all the reported observations. Side-lobe effects are evident on synthesized range-height displays and make it a difficult task to deduce the true vertical thickness of the echoes. Values as small as 2.5 km have been deduced but the general range reported is 5-20 km. In spite of the smearing, however, there does seem to be considerable structure in the echoes and more of this is seen as shorter

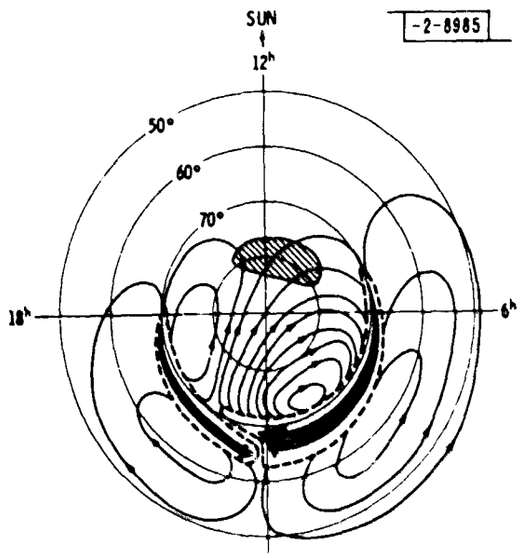

Fig. 4-1. Illustrative pattern of ionospheric electric currents causing magnetic ray disturbances in auroral zone and associated currents at higher and lower altitudes. Shaded area near 80° magnetic latitude locates approximately a region of enhanced daytime field fluctuations. (After Sugiura and Heppner, 1965.)

pulse lengths are used.

Many workers have classified their echoes into "diffuse" and "discrete" depending on whether patchiness is seen, but the time variability, horizontal displacements, and system characteristics are all involved in these definitions so that a clear-cut comparison between the two terms has little meaning when comparing different workers' results. The apparent positions and measures of off-perpendicularity are also strongly influenced by the beam-widths, the corrections for refraction applied and even the strength of the magnetic field perturbation, as that too many alter the position in space of optimum echo occurrence. In general, however, the echoes appear to be field-aligned, to originate from fairly narrow layers in the E-region, and to accompany auroral electrojet currents.

A general survey of where these echoes may occur with respect to geomagnetic latitude and local time has recently been given by Hartz (1968) and is reproduced in Fig. 4-2. Echoes occur most frequently in the evening sector for the so-called type A_2 echoes which are observed in the 110 km region; Hartz also illustrates the occurrence of type A_3 echoes, which some workers assign to an altitude near to 85 km although this has not been proved, and these exhibit a maximum around 0400. Most such diagrams could be interpreted on the basis of a physical link to the auroral electrojet current. In addition the occurrence of visual aurora as portrayed in Fig. 4-3 from Stringer and Belon (1967) follows the same general pattern. One would not, of course, expect a one-to-one correspondence between visual and radio aurora, even if they had a common origin, because of the magnetic geometry conditions discussed above.

Many workers have noted a relationship between geomagnetic disturbances, as monitored by local or planetary K indices, and radio aurora. Again the auroral electrojet current seems to be the intervening link. For some stations very high K values are accompanied by a low radio auroral occurrence probability and this is probably due to the movement equatorwards of the strong current core so that the aspect angles are not favorable. This movement is such that radar systems located at temperate latitudes see radio

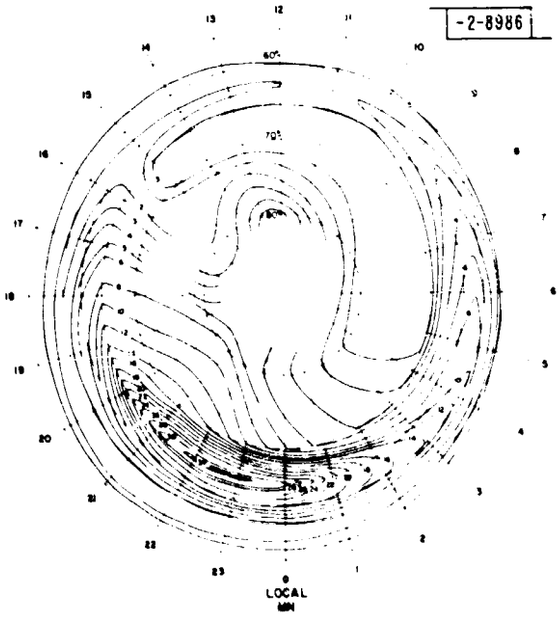

Fig. 4-2(a). Percentage of time that type A_2 radio aurora occurred in 1959-1961 on VHF propagation circuits in Northern Canada. Data are plotted as a function of geomagnetic latitude and mean geomagnetic time appropriate for midpoint of path. (After Hartz, 1968.)

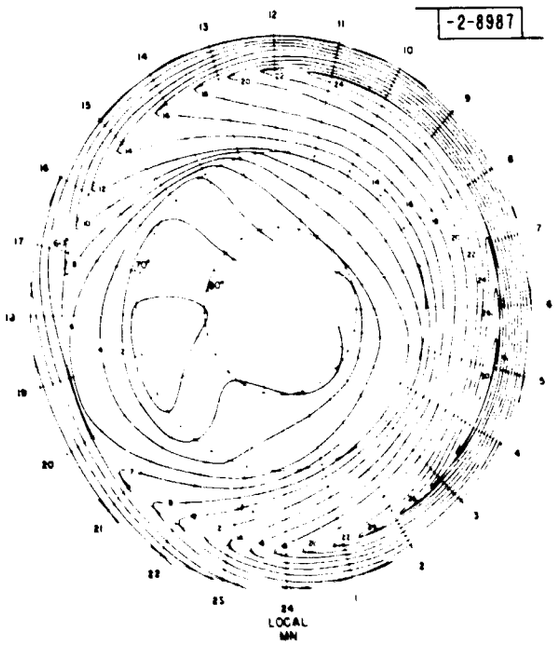

Fig. 4-2(b). Percentage occurrence of type A_3 radio aurora recorded in the same way as in Fig. 4-2(a). (After Hartz, 1968.)

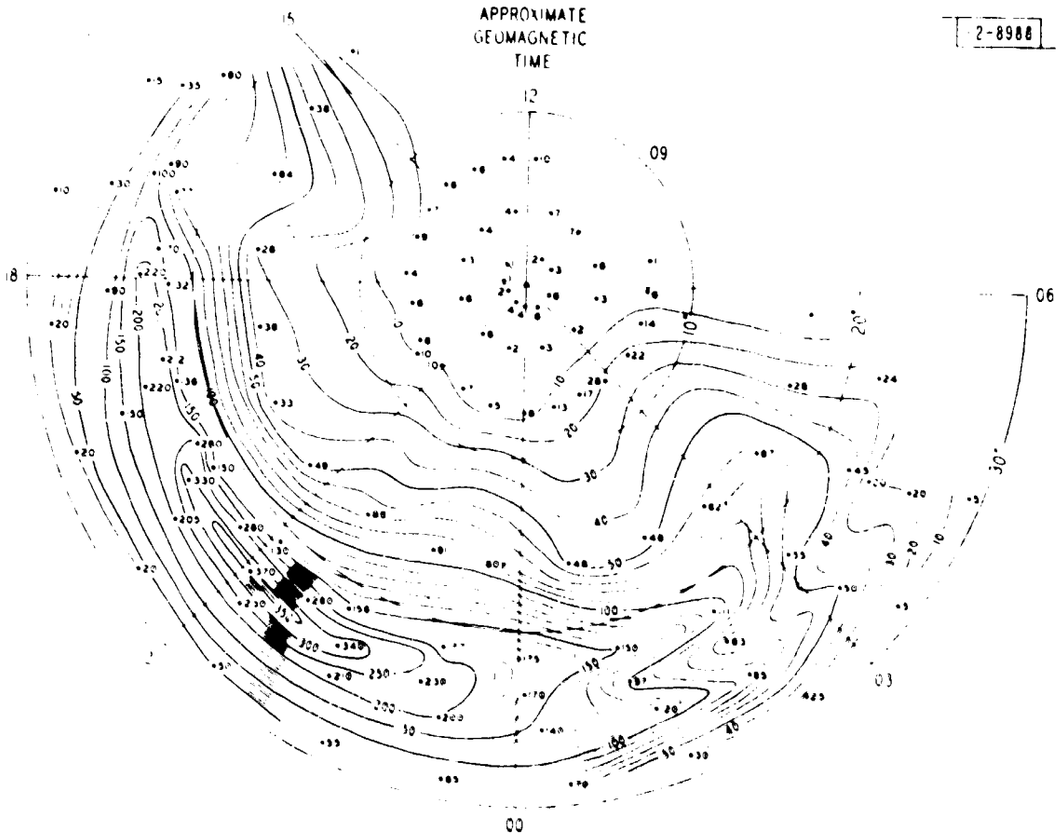

Fig. 4-3. IGY isoauroral diagram for discrete auroral forms. Contours of equal auroral incidence plotted on arbitrary scale against dipole colatitude. (After Stringer and Belon, 1967.)

aurora at higher elevation angles and closer ranges during moderately disturbed conditions more often than during low Kp conditions. Complicating the comparisons is the fact that the planetary magnetic disturbance index Kp is used by many workers, because no local measure of disturbance is available; it would be preferable to use a parameter derived from magnetometer observations near to the electrojet such as the auroral electrojet index.

The longer term variability of radio aurora reflections, like that of geomagnetic disturbances, shows a semi-annual variation (not always well marked) and a tendency for a sunspot cycle variation. There have been very few efforts to monitor these variations with a given system and there is a singular lack of quantitative volume reflectivity measurements that would be required to form a basis for such studies.

Information is also meager on the shorter time variability and it is hoped that this may be rectified in the current study (see Section 6 C below). There have been claims of pulsating echoes associated with magnetic sudden commencements but whether a spatial or time variability dominates these results is not clear.

C. Wavelength Dependence

The most comprehensive experimental studies of this aspect of radio aurora are those by the Stanford Research Institute group in the 50-3000 MHz range. The echo intensity varies roughly as λ^7 in the 1000-3000 MHz range but only as about λ^3 in the 100-1000 MHz range. There appears to be a continuous gradation of the wavelength power with frequency. The Stanford work uses the same pulse length at all frequencies and corrects the signal intensity at longer wavelengths to account for the fact that the beams are only partially filled. The assumptions made in this correction then become crucial; one set used has been that the echoing region is about 16 km thick and of unlimited azimuthal extent. The pulse length smearing is also an important factor in deducing absolute volume reflectivity and one set of observations at Millstone using alternate 500 and 100 μsec pulses yielded absolute reflectivity values some 5-6 db greater with the shorter pulse length.

D. Observed Velocities

Velocity can be derived in two ways: from range variations of echo features and from Doppler shift measurements. Agreement between the two approaches cannot be expected always as the former includes false velocities produced by echo development and changes. The velocities found are generally towards the west before midnight and towards the east after midnight, corresponding to the drift of auroral forms. This pattern is consistent with the classical current pattern of Fig. 4-1, provided the observed velocities are in the same direction as the electron velocities as discussed below. This agreement provides evidence in favor of the classical current picture rather than the modification introduced by Akasofu et al. (1965) in which the current is directed westwards before and after midnight. The values for the velocity deduced are generally several hundred meters per second. According to Millstone results, the velocity pattern also depends on altitude (see below) and varies within the echoing region; these features have yet to be fully explored. Away from the magnetic meridian the Doppler velocity tends to become independent of azimuth, suggesting a constant phase velocity for the scatterers, rather than varying with azimuth as might be expected for a drifting irregularity. The width of the spectrum is also subject to control of the beam-width pulse-length smearing factor as can be seen from the occurrence of very wide spectra close to the meridian, and again more detailed measurements are required.

E. Theoretical Interpretation

Initially the radio auroral echoes were interpreted as anisotropic drifting irregularities produced by turbulence. Later, by analogy with the theories used to explain irregularities in the equatorial electrojet, they were interpreted as longitudinal electrostatic waves set up in a region of strong current flow by a two-stream plasma instability. The latter theory has two forms so far as expounded by Farley (1963) and Kato and Hirata (1967). The two-stream theory predicts that when the electron-ion relative velocity in a plasma exceeds the ion thermal velocity by a certain factor, unstable waves can grow and propagate. Propagation is perpendicular to the field lines and in a general direction opposite to the current vector. The waves effectively bunch the

electrons as in a travelling wave tube; the conductivity along the field lines is much greater than that transverse and the wave fronts are thus field-aligned.

The two-stream instability theories developed thus far involve the use of small perturbation linear assumptions and predict the conditions under which waves may grow, the phase velocity at the threshold of growth and the rate of growth, but can give no information on the amplitude of the waves and thus on the intensity of the reflected signals as a function of wavelength. A radar has a maximum response to those waves whose wavelength is one-half of the radar wavelength and while a family of wavelengths may be excited, simultaneous measurements at a number of frequencies are required to establish the partition of energy between the waves in situ. Farley's theory predicts that the critical electron drift velocity required for wave growth increases as the irregularity wavelength decreases. For a given drift velocity therefore, the growth criteria may be met for long waves but not for short waves. Kato and Hirata give considerable emphasis to the growth rate of the waves. For a given electron drift velocity they present dispersion curves from which one may deduce the maximum growth rate. For an electron velocity of about 1000 $msec^{-1}$ this growth rate occurs at a wavelength of about 11 cm and is thus near to the optimum wavelength detectable by Millstone. The growth rate itself is of the order 200 μsec, i.e., much faster than the sampling rate. The observed wavelength dependence must therefore be a manifestation of i)the reflection characteristics of the waves themselves (for plane waves a λ^4 dependence would be expected) and ii)the relative abundance of waves of different wavelength (which is governed partly by the electron drift velocity and the growth rates). The interacting factors remain unexplored.

The evidence favoring the two-stream instability theory over the turbulent irregularity theory has recently been reviewed by Abel and Newell (1969) (Sec. 6 A). The Doppler data obtained at Millstone provides supporting evidence for the theory. Also a rotation with altitude of the vector describing the wave motion is found which is similar to the manner in which the

current vector rotates. The magnitude of the Doppler velocity, typically 400-500 m sec is close to that predicted by Farley.

The expectation of a rotation of the current vector with altitude can best be explained in terms of the following example. In the evening sector an electric field of about 50 mv/m may exist directed northwards. At about 110 km the mobilities of the electrons and ions are such that the electrons would drift westwards in response to this field with a velocity of about 1000 $msec^{-1}$ while the ions drift towards the NNW with a velocity of about 300 $msec^{-1}$. The differential velocity or the current vector (by definition) points towards the ENE. The current itself exists because of the mobility difference. At higher levels, say 150 km, both electrons and ions drift together towards the west at about 1000 $msec^{-1}$ (because both electron and ion gyrofrequencies exceed their collision frequencies with neutral particles) and there is little resultant current. At levels just below 110 km the electrons may drift in response to an applied field, but the ions are constrained to move with the neutral medium. The electron concentration is low and again the total current is small. At still lower levels, say less than 50 km, both electrons and ions move with the neutral medium.

The largest currents occur in the 100-120 km layer and it is here that the criterion for electrostatic wave growth can be met. The electron-ion relative velocity exceeds the ion thermal velocity by the required factor. The ultimate energy source for the waves is the applied E. M. field as in a travelling-wave tube. This electric field provides kinetic energy to the electrons and as they stream through the ions some of the kinetic energy goes into the potential energy inherent in the charge distribution in the waves.

Kato's theoretical results illustrate nicely that when the ion thermal velocity is increased, the waves are damped, essentially because the collisional diffusion process which destroys the charge gradients is accelerated. Thus ion temperature is a critical parameter. At lower levels one might expect the higher collision frequencies to play an analogous role to high ion temperatures

but the dispersion relations have not been worked out yet for D-region conditions. Indeed the range of variables selected for the theoretical work to date needs extension to completely encompass conditions in the auroral zone.

5. UHF Refraction Experiment

A. Plan

i) General

As outlined in Section 3, both systematic and time varying refraction effects can be expected at UHF induced by the ionosphere and the neutral atmosphere. Measurements of the combined effects will be valuable in establishing limitations on the tracking accuracy of defensive radars operating at UHF, but may not necessarily be of guidance concerning the accuracy expected at other frequencies, since only the ionospheric effects are frequency dependent. Accordingly it is planned to make simultaneous measurements at UHF (400 MHz) and L-band (1295 MHz). For the former passive lobe-comparison tracking of satellite beacons will be employed, while for the latter monopulse radar skin-tracking will be used. Comparison of arrival angles at these two frequencies should yield separately the ionospherically induced refraction effects while an absolute comparison of the L-band observed and predicted positionsshould chiefly yield the atmospheric refraction.

This section describes in greater detail various aspects of this work. Broadly speaking, however, the measurement of the refraction effects must proceed in two steps discussed below,namely the calibration of the antenna to determine repeatable pointing errors of instrumental origin and the subsequent program of active measurements on satellites.

ii) Systematic Pointing Errors

In order to compare absolute positions at L-band with predicted positions it is necessary to calibrate out a large number of sources of systematic error, including for example, deformations of the dish structure with elevation. In order to do this a scheme involving the multibeam tracking of radio stars (at L-band) has been devised and is discussed in part 3) of this section. In process of calibrating the antenna pointing it is of course necessary to assume models for the tropospheric refraction. Currently the models employed are based upon ray tracing calculations per-

formed for different values of the refractivity at ground level. Methods of improving these models are also discussed in section 5 F.

Figure 5-1 summarizes the determination of the systematic pointing errors in the manner outlined above. This work does not depend upon the UHF tracking capability and has therefore already begun, but must be repeated when the new subreflector is in place. The procedure employed is to point the antenna continuously (via a digital computer) and sample the monopulse error voltages for storing in the computer. A limitation at present is the $.011^{\circ}$ detents in the shaft encoder positions. It is planned, however, by installing new resolvers to reduce this to $.003^{\circ}$. The calibration of the error voltages as a function of angle offset can readily be accomplished by performing repeated programmed scans across the source.

Passive tracking will also be performed at UHF in order to ensure that the axes of the beams at UHF and L-band are colocated.

iii) L band active tracking of satellites

The UHF/L-band tracking system is described in Section 5 C and the performance expected in 5 D. A number of steps are being taken in order to ensure that the L-band radar performs adequately when skin-tracking satellites to low elevations. These include replacing the shaft encoders as noted above, and performing a program of satellite tracking to determine the tracking accuracy under dynamic conditions. The plan of work involved here is outlined in Figure 5-2. It is anticipated that the tracking accuracy of the system can be determined from a comparison of the instantaneous azimuth α and elevation angles β with the computed values α' and β' to yield an rms tracking accuracy ξ given in

$$\xi = \sqrt{[(\alpha - \alpha')\cos\beta]^2 + (\beta - \beta')^2} \qquad (5\text{-}1)$$

Here the instantaneous position α, β will be obtained by adding algebraically the shaft encoder positions and the monopulse error voltages calibrated in terms of an angular offset. The expected positions α' and β' can be determined by fitting an orbit to the observed satellite range, doppler and

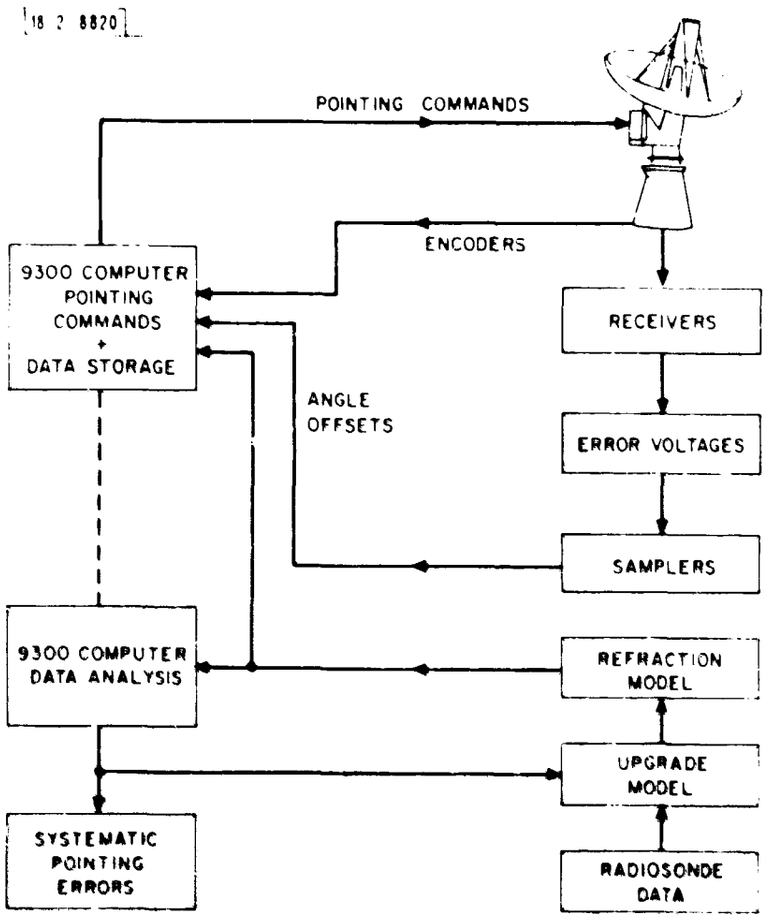

Fig. 5-1. Procedure for calibrating repeatable pointing errors in system from observations of positions of radio stars.

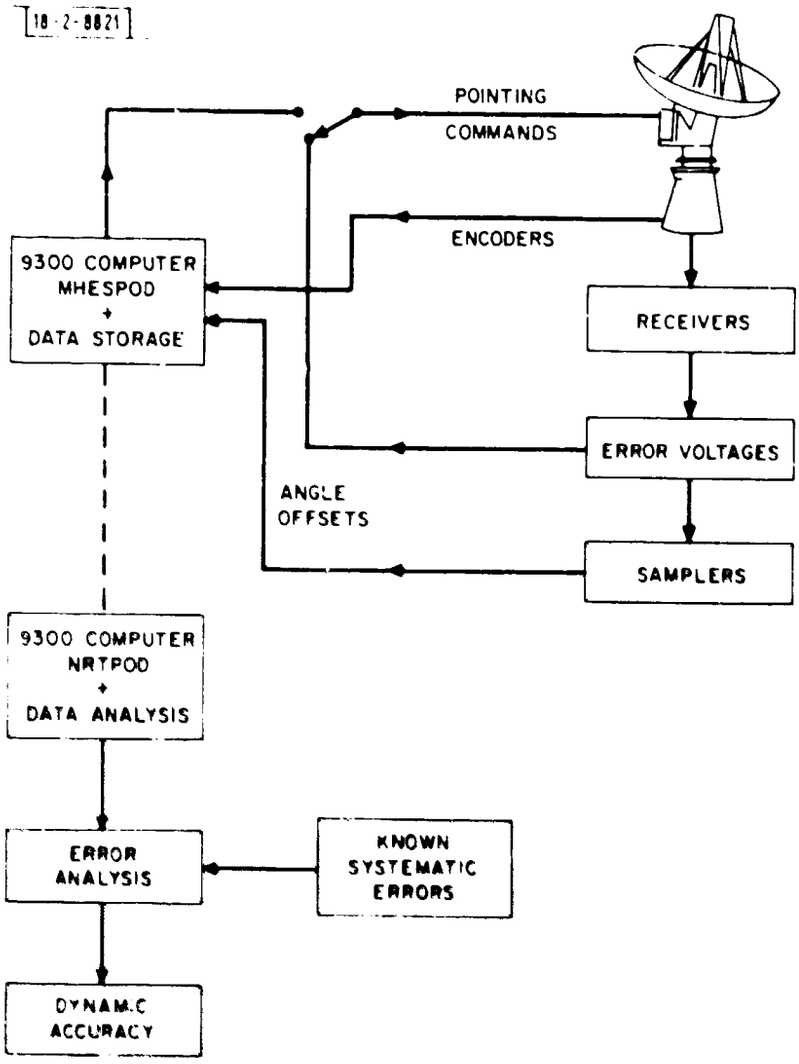

Fig. 5-2. Method of determining dynamic tracking accuracy via active satellite tracking.

angular positions using a Non-Real Time Precision Orbit Determination (NRTPOD) computer program available at Millstone. This program is useful in solving for biases and in making statistical analyses of the observational residuals, in addition to its prime capability of precisely updating orbital parameters.

The determination of the rms tracking error ζ is needed in order to establish the level of the least detectable angular scintillation, i.e. a lower bound on short-lived tropospheric effects.

At low elevations where the most pronounced refraction effects occur reliable closed-loop tracking may not be possible, either because of these effects or because the signal-to-noise ratio will be poor. In this event it will be necessary to compute the expected position of the target and use the computer to direct the antenna. This can be accomplished using another of the Millstone programs, MHESPOD[1], which has the capability of running in real time. This program generates an updated steering ephemeris which fits the observations currently at hand within 30 sec of an operator request. Between updates, computer-steering of the antenna is available from the last ephemeris generated. MHESPOD's real-time orbit-fitting and steering functions are directly applicable to the study of propagation at low elevation angles. Smooth computer-steering based on the trajectory extrapolated from fitting "clean" observations at higher elevation angles would avoid possible problems of poor auto-track performance near the horizon.

Both NRTPOD and MHESPOD are capable of initialization from a position-velocity state-vector if very accurate pre-run trajectory information should be available, otherwise initial conditions can be derived from SPADATS mean elements. The steering ephemeris is then generated by numerical integration of the corresponding trajectory, subject to a sophisticated force-model which may be redefined by the user.

In the event that it proves impossible to track all targets of interest at low elevations without employing computer steering of the

1 Millstone Hill ESPOD where ESPOD is an Air Force Electronic Systems Division Precision Orbit Determination program, i.e. a special perturbations program for differential corrections of initial conditions by weighted least-squares minimization of residuals.

antenna additional computer programming will be required in order to include in the machine at the same time MHESPOD (or some simpler version) together with the data acquisition program.

B. Monopulse Error Tracking Calibration

As noted earlier the tracking characteristics of the Millstone antenna are currently being studied through the observation of radio stars. Certain radio stars are very convenient for this purpose because they are small with respect to the antenna beamwidth, have constant power output and have precisely predictable orbits through the sky. The signals are wide-band gaussian noise, the intensity of which is usually described in terms of an antenna temperature, T_A, defined by

$$P = kT_A B \quad \text{watts.} \tag{5-2}$$

where

P = received power

B = Receiver bandwidth (Hz)

k = Boltzmann's constant

The uncertainty in the measurement of the antenna temperature for a receiver temperature T_R and integration time τ is

$$\Delta T = \frac{T_R + T_A}{\sqrt{B\tau}} \tag{5-3}$$

The uncertainty in the measurement of the angle of arrival of the signal, using the monopulse error channel response can then be shown to be

$$\Delta\theta = 0.4 \frac{\theta_o}{\sqrt{B\tau}} \frac{T_{eff}}{T_A} \tag{5-4}$$

where

$$T_{eff}^2 = T_A T_R + T_R^2$$

θ_o = beamwidth of the antenna

The sensitivity can be great if $\sqrt{B\tau}$ can be made large, and for Millstone it is typically 10^4. At L band, the source Cassiopeia A yields an antenna temperature for the Millstone antenna of $T_A = 200^{\circ}K$, and the receiver temperature T_R is such that $T_{eff} = 280$, giving $\Delta\theta/\theta_o = 0.01\%$

The principal radio sources used in this work are listed below with their antenna temperatures, diameters and declinations.

SOURCE	T_A (1295 MHz) (^oK)	T_A (400 MHz) (^oK)	Diameter (arc min)	Declination (^{o})
CASSIOPEIA A	205	460	4	59
CYGNUS A	135	340	2	41
TAURUS	84	91	4	22
VIRGO	15	44	5	13
ORION	38	17	6	-5

The radio star observations are expected to fulfill three objectives: (a) generate pointing correction tables for the antennas at both 1295 and 400 MHz, (b) check accuracy of the low angle tropospheric refraction models (c) investigate instrumental effects such as wind loading on the antenna, ground reflections, encoder granularity, etc.

To implement this program, wide-band phase detectors have been installed to improve the sensitivity. A special computer program for the SDS 9300 computer has also been written which commands the antenna in various scanning routines and accepts and analyzes data from the receiver. The antenna control system is shown in Figure 5-1 . The computer program is essentially complete and systematic data gathering will begin soon.

Samples of the receiver outputs are shown in Figure 5-3 with the antenna scanning Cassiopeia A in elevation under computer control. The azimuth channel deflection is due to the azimuth pointing error. To generate the pointing correction table a standard scan routine is executed on sources over a wide variety of azimuth and elevation angles. The source is scanned in elevation and azimuth over a 5° angle at a rate of

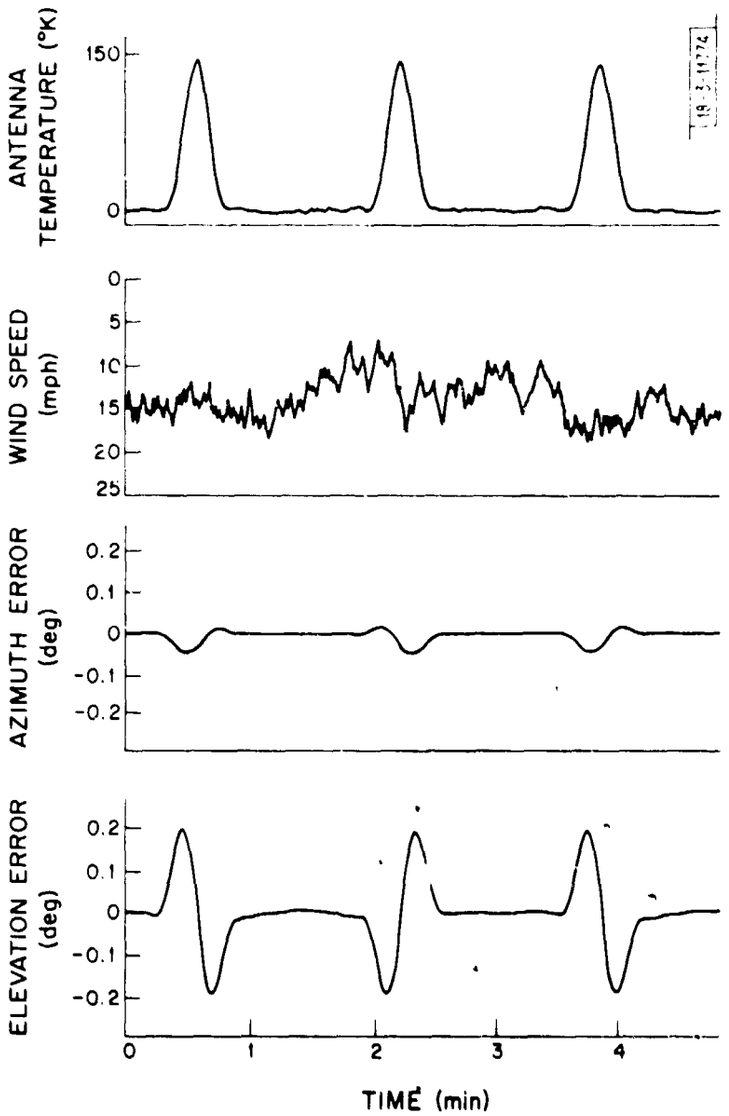

Fig. 5-3. Samples of receiver sum and error channels when performing forced scans in elevation across source Cassiopeia A.

2°/ minute. The computer finds the apparent coordinates of the source in two ways. It finds the scan centers first by determining the half power points of the on-axis response, and secondly by determining the location of the zero crossings of the error channel responses. It is important to note that both methods have the same intrinsic accuracy. Interestingly, systematic discrepancies have been found between the two methods.

The pointing program presently includes a tropospheric refraction model based on data supplied by R. Crane, in which the refraction is estimated only on the basis of the ground refractivity. It is hoped to upgrade the model (Sec 5F) and the accuracy of the existing or any improved models will be checked.

While the monopulse feed system is not better than a single horn feed for determining pointing biases it is extremely useful in studying the instantaneous apparent angle of arrival of signals. For example, Figure 5-4 shows the result of tracking Cassiopeia A near transit where the elevation rate is very low. The basic saw-tooth pattern in the elevation error plot (bottom graph) is due to the granularity (0.011°) of the existing shaft encoders.

The signal reflected off the ground into the antenna has also been seen interfering with the direct signal at very low elevation angles. The effect is noticeable mainly below 1° elevation in the elevation error channel.

C. UHF/L-band Tracking System

The Millstone L-band radar system is being modified to include a UHF monopulse receiver. A frequency selective subreflector with a UHF feed will replace the present Cassegrain subreflector to permit simultaneous L-band radar and UHF beacon tracking of a transmitting satellite (Sec. 2 B).

The control for the antenna will be provided by the L-band tracking system shown in Figure 5-5. The L-band system will also provide the range information via the Sequential Doppler Processor (SDP). The primary application of the UHF receiver will be to derive precision angle measurements. Signal strength measurements will also be made to help determine the

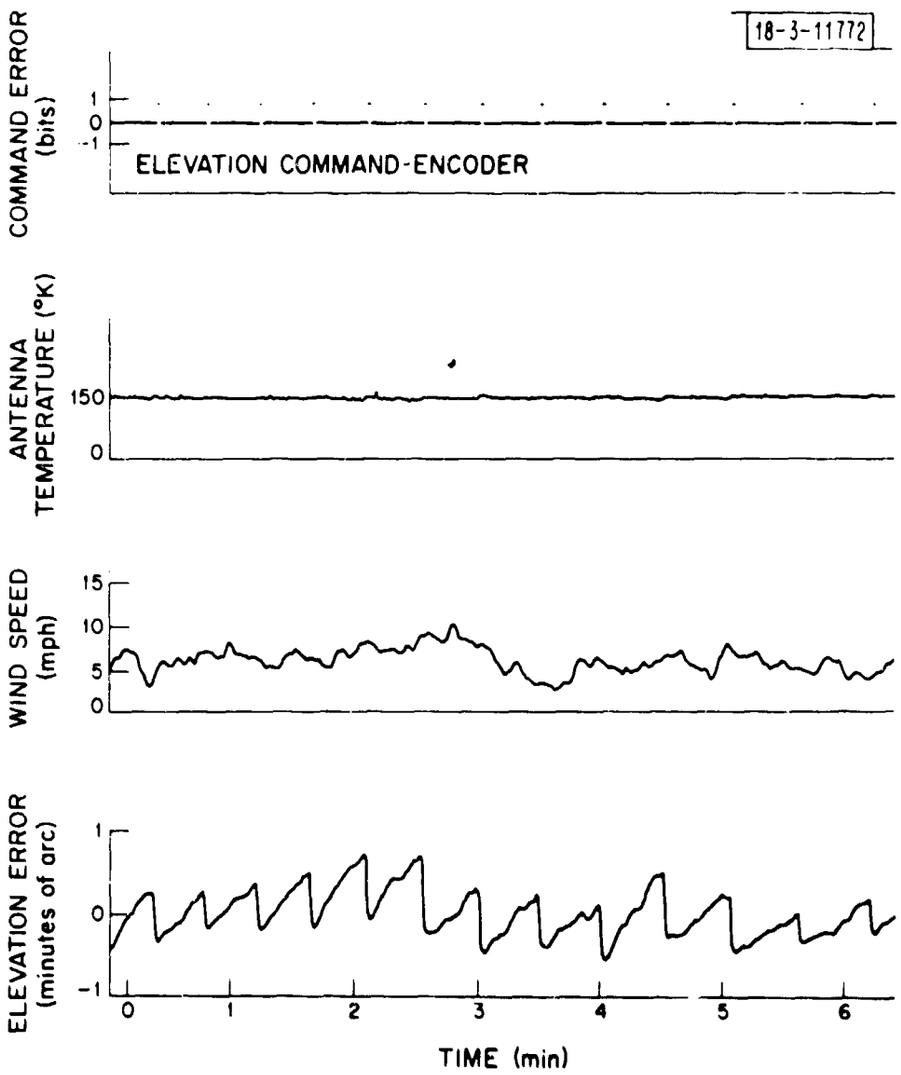

Fig. 5-4. Results of monopulse tracking Cassiopeia A near transit. Saw-tooth error voltage pattern results from 0.011° granularity of encoders (top channel). Note also some correlation with wind speed.

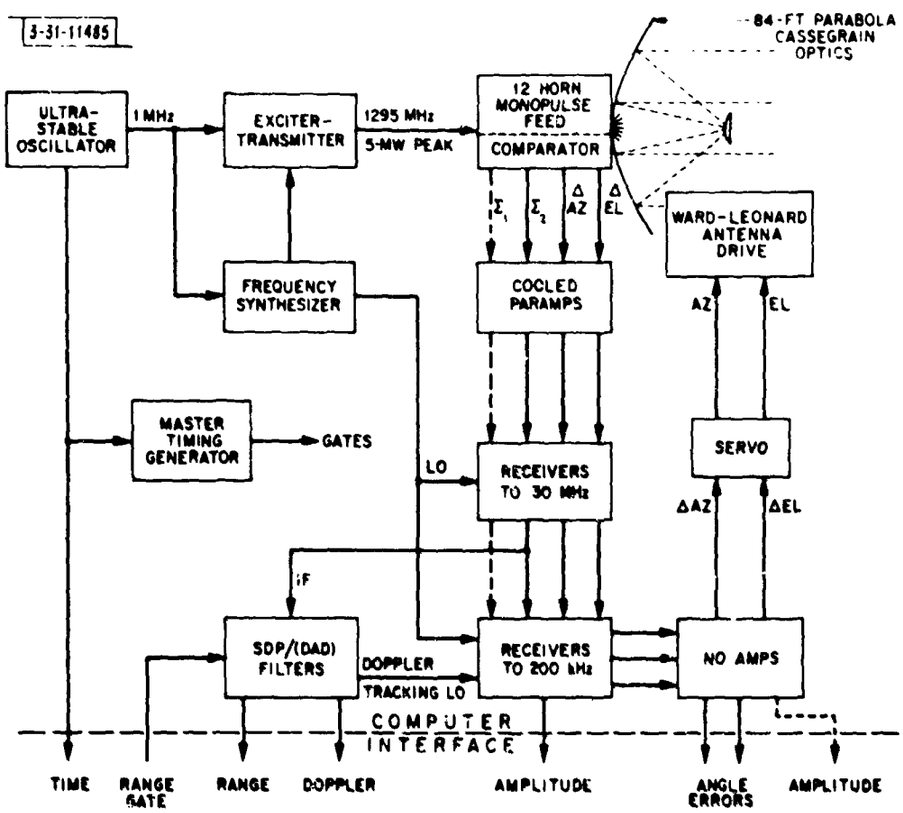

Fig. 5-5. Block diagram of L-band radar tracking system.

amplitude scintillation characteristics of the propagation medium.

The UHF feed will consist of crossed-dipole elements followed by a comparator-polarizer unit. The feed will be located at the prime focus of the antenna. Left and right circular polarization outputs from the polarizer will be available for input to the UHF receiver. The orthogonally polarized 'sum' signal will be used in a fourth channel of the UHF receiver which will be assembled with components procured for spare parts.

A characteristic of the Transit satellites that will be used for some of the refraction experiments is the transmission of a VHF beacon signal (nominally 150 MHz) which is phase coherent with the UHF beacon (nominally 400 MHz). Therefore an additional channel at 150 MHz will be assembled to provide data for the dispersive doppler experiment (discussed in part E of this section). The UHF and VHF beacon signals are offset in frequency by 80 parts per million. The configuration of the UHF/VHF receiver system shown in Figure 5-6 makes use of the offsets to provide the final IF frequencies and this in turn provides an easy means of recovering the dispersive doppler data as well as fulfilling the design requirements for the UHF receiver.

The sensitivity of the RF amplifier and performance of the tracking filter will determine, to a large extent, the overall receiver characteristics. The RF section of the receiver will have low-noise transistor preamplifiers. RF losses are expected to occur in the components that must be used for protecting these amplifiers against the L-band radar and for inserting calibration signals. The receiver noise temperature is expected to be approximately 500°K. The tracking filter incorporates a 3rd order phase-lock loop with selectable loop bandwidths (3-300 Hz) to provide precise tracking of a variable carrier frequency. The nominal bandwidth which will be used is 10 Hz, which will yield an overall system noise power of -162 dbm. All receiver components have been specified to have $\leq \pm 1$ db gain variation and $< 5^{\circ}$ relative phase shift between channels. All local oscillator frequencies are generated by frequency multiplication from the 1 MHz station standard to ensure phase coherence between receivers.

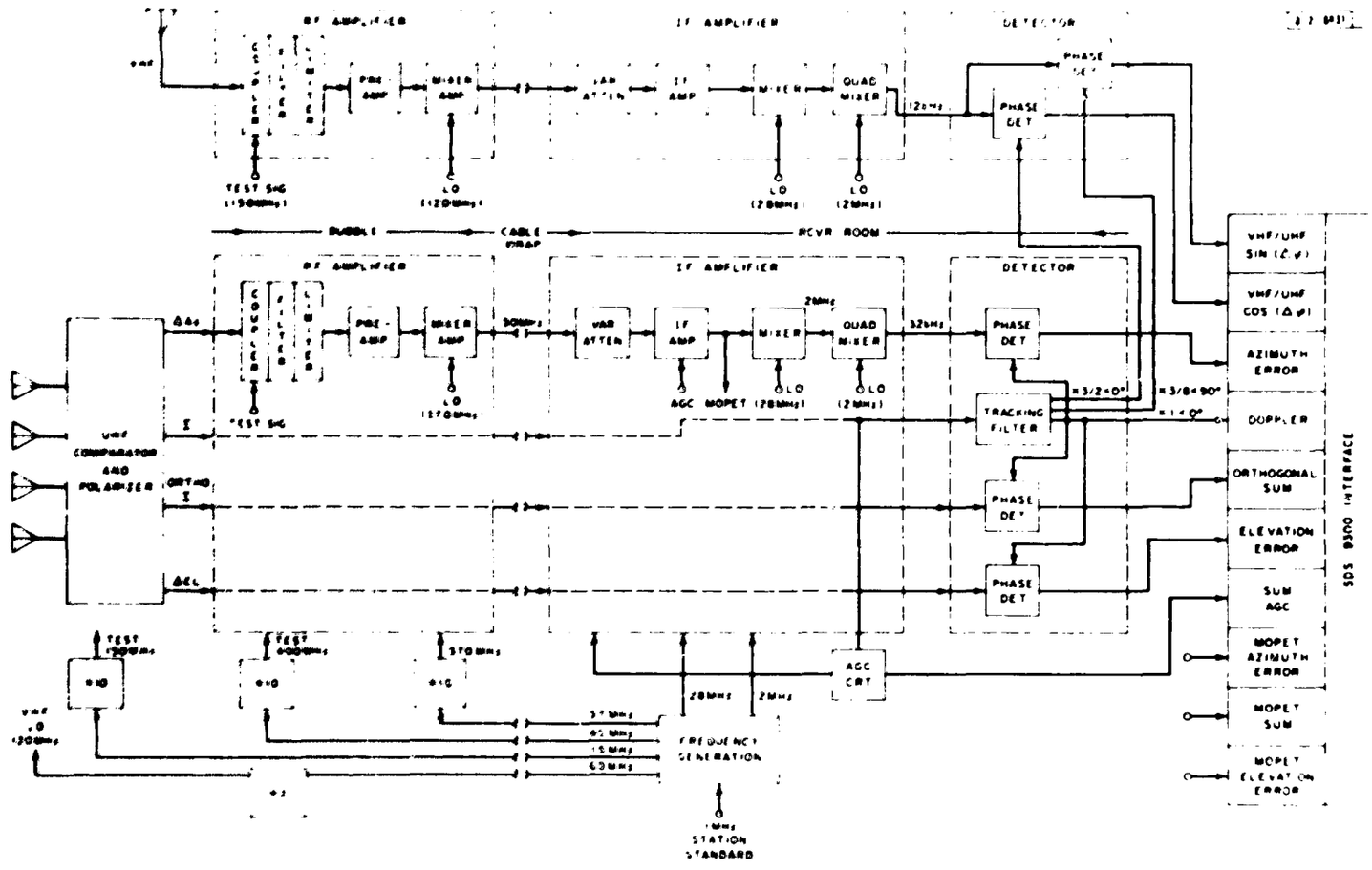

Fig. 5-6 Block diagram of the UHF receiver system.

The RF amplifier and 1st conversion stages will be housed in a remote environmental enclosure (bubble) located at the antenna feed (See Fig. 2-3). The IF signals, test signals, and local oscillator frequencies will be transmitted via coaxial cable to the main receiver room where the IF amplifiers are to be located. The 30 MHz IF signals are then converted to the 80 p./million offset frequency, and the 'sum' signal will be applied to the tracking filter. The locked-oscillator output of the tracking filter is then applied to the detectors of the off-axis channels of the UHF receiver to produce the desired angle information voltages. The various data inputs to the SDS9300 computer are shown in block diagram of Fig. 2-4.

D. UHF/L Band Observations

As discussed in earlier sections it is proposed that satellites in the Navy Transit series be skin-tracked by the 1295 MHz radar while the 400 MHz CW transmission from the on-board transmitter are also received. The principal parameters of this instrumentation are set forth in Table 5-1. There are usually 4 of the Transit series satellites in polar orbits at all times. The altitudes are about 1000 km so that at 400 MHz the doppler shift is confined to a 10 KHz window and the doppler rate is ≤ 6 Hz/sec. The beacon provides a 1 watt signal transmitted isotropically, which is circularly polarized at high elevation angles and linearly polarized at low elevation angles.

The orbit of the satellite on each pass may be established in real-time from the radar observations of azimuth, elevation, range and range rate at high elevation angles so that the antenna can then follow the satellite as it sets under computer control (Sec. 5 A). The power received at 1295 and 400 MHz from the radar and beacon will be respectively

$$P_R(1295) = \frac{P(\text{transmit})}{4\pi R^4} \frac{A^2 \sigma}{\lambda^2} \qquad (\text{Radar}) \qquad (5\text{-}5)$$

$$P_R(400) = \frac{P(\text{beacon})}{4\pi R^2} A \qquad (\text{Beacon}) \qquad (5\text{-}6)$$

Table 5-1

MILLSTONE RADAR FACILITY, INSTRUMENTATION FOR PROPAGATION STUDIES

	L-Band Tracking Radar	UHF Tracker
Frequency	1295 MHz	400 MHz
Transmitter Power	150 KW ave/5 MW peak	NA
Pulse Length	10-4000 μsec	NA
PRF	≤ 50 PPS	NA
Duty Factor	3%	NA
Receiver		
System Temperature	~ 150°K	~ 500°K
Bandwidth	Matched to 2 m sec pulses	3-300 Hz
Antenna		
Collecting Area	210 m^2	~ 200 m^2
Gain	47 DB	~ 37 DB
Beamwidth	0.7°	~ 2.36°
Feed	12-horn monopulse array	Monopulse
Polarization	Circular	Circular

where

$P_{transmit}$ = transmitter power

R = range

A = antenna collecting area

λ = wavelength

P_{beacon} = satellite beacon power

α = satellite cross section

Adopting a value $R = 3.7 \times 10^6$ m (satellite setting) and $\alpha = 1 m^2$ one finds P_R (1295) = 1.8×10^{-15} watts and P_R (400) = 1.2×10^{-12} watts for a 1 watt beacon transmitter. For a strong signal the uncertainty in the angle of arrival measurement is approximately

$$\Delta\theta \cong \theta_o \sqrt{\frac{kTB}{P_R}} \tag{5-7}$$

where

θ_o = beam width of antenna

kTB = receiver system noise power

Assuming a filter matched to the 2 ms pulse length employed for radar tracking at 1295 MHz and a 10 Hz bandwidth for the UHF receiver we obtain when averaging over a period of= 1 second

$$\begin{aligned} \Delta\theta\ (1295) &= 0.25' \\ \Delta\theta\ (400) &= 0.01' \end{aligned} \tag{5-8}$$

From this analysis it would seem that a high elevation angles where refraction effects are small UHF beacon tracking may be intrinsically more accurate than that provided by the L-band radar and provision is being made to permit auto-tracking by either method.

E. Dispersive Doppler Experiment

The Navy satellite beacons transmit coherently on 400 and 150 MHz. The transmitter frequencies are offset from their nominal values by 80 parts per million (Sec. 5 C). Because the wavelength dependence of the index of refraction for an ionized medium is known (Eq. 3-5), the total electron content can be inferred by comparing the phases of the two received signals. (See for example Arendt et. al. 1965) As discussed in Section 5 C, the 400 MHz and 150 MHz signals will be converted to 32 and 12 KHz respectively.

The 32 KHz 'sum' signal will then effectively be multiplied by 3/8, and combined with the 12 KHz signal in quadrature phase detectors. The phases of the two signals are

$$\Phi_{400} = \Phi_T + \Phi_{I_{400}} \tag{5-9}$$

$$\Phi_{150} = \Phi_T + \Phi_{I_{150}} \tag{5-10}$$

where

$$\Phi_T = \frac{2\pi}{\lambda} \int n_T dr$$

$$\Phi_I = \frac{2\pi}{\lambda} \int n_I dr = \frac{2\pi}{\lambda} \int [1 - \frac{N_e e^2}{2\pi m f}]^{\frac{1}{2}} dr$$

Φ_T = tropospheric phase shift

Φ_I = ionospheric phase shift

N_e = electron density

f = frequency

λ = wavelength

m = electron mass

r = ray path

e = electronic charge

If the propagation paths are assumed to be identical, i.e., differential refraction is ignored, then the difference between the phases of the two signals will yield

$$\Delta\Phi = \Phi_{150} - \frac{3}{8}\Phi_{400} = -\frac{55}{64}\frac{e^2}{mcf}\int N_e dr \tag{5-11}$$

Under quiet ionospheric conditions $\int N_e\, dr$ varies smoothly with time whereas in disturbed conditions it can vary erratically. The correlation between the total electron content and scintillation activity during

aurora will be investigated in this program.

F. Theoretical and Analytical Study of Refraction

i) Improved Models for Tropospheric Refraction

As noted in Section A above the problems of determining all possible sources of systematic pointing error and tropospheric refraction effects are inseparable. We propose to proceed on the assumption that all biases in the system are repeatable. Thus, day to day variations must be attributed to departures of the tropospheric refraction from that assumed in the initial models.

The problems of refraction at low elevations caused by the lower atmosphere have been discussed in Section 3. Currently the antenna pointing programs being utilized for radio star tracking (Section 5 B) employ a fixed model for the atmospheric refraction. In an effort to upgrade the model the effects of synoptic scale changes are being studied by ray-tracing techniques. A large number of ray tracings have been performed for elevation angles between 0.1° and 90° using data from the Albany, N.Y. radiosonde station. The elevation bending and range errors were computed for each elevation angle for each of the 0000 and 1200 GMT radiosonde soundings for the months of February and August for the years 1966, 67 and 68. A scatter diagram for a 1.0° elevation angle is shown in Figure 5-7. This data is being statistically analyzed to look for yearly, monthly, and hourly dependences.

The deviation of the atmosphere from one descriptable by horizontal homogeneity is also being investigated. A ray tracing program is being utilized that calculates the elevation and azimuth bending and range errors for given three-dimensional distributions of the index of refraction. Computations of the azimuth and elevation angle dependence of these errors are being computed for models of the horizontal change in refractive index in the troposphere determined by the use of three or more simultaneous radiosonde profiles taken several hundred miles apart.

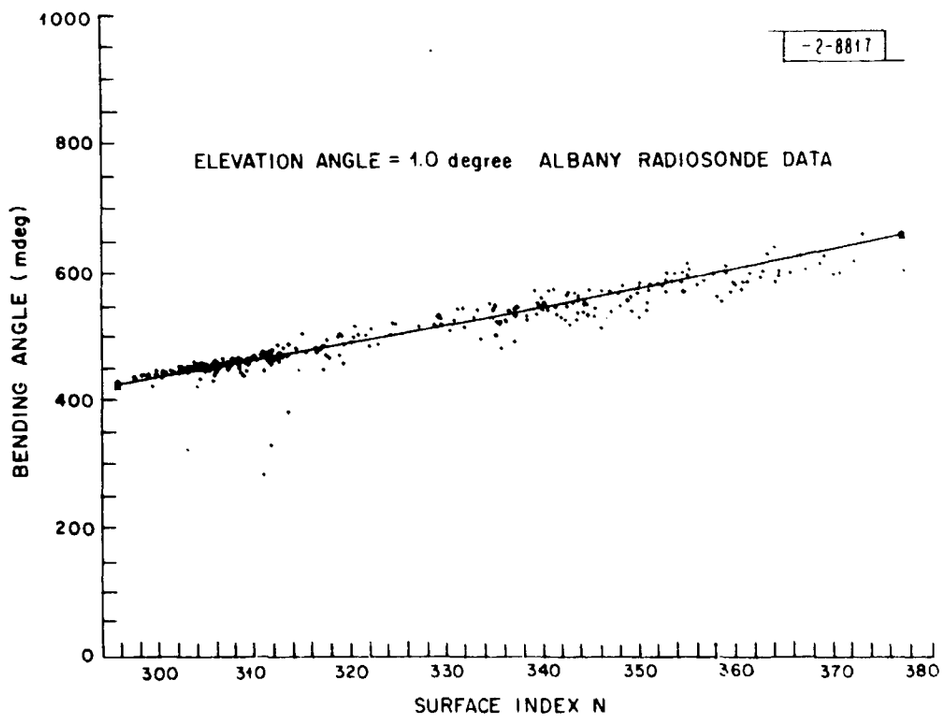

Fig. 5-7. Total bending in elevation (in millidegrees) for elevation of 1.0° computed by ray tracing for refractivity profiles obtained at Albany, N.Y. vs refractivity at surface.

ii) Analysis of the Ottawa Trough

A persistent feature of the nighttime ionosphere along the southern border of Canada is a trough of low ionization that was first recognized from Alouette observations and has become known as the 'Ottawa trough'. In order to investigate the effect of this phenomenon for a frequency of 400 MHz a scalar model of the refractivity (in N units) was made based upon published electron density profiles. This model is shown in Figure 5-8. East-West symmetry was assumed when calculating the angle deviations for a ray traversing this feature and the results are shown in Figure 5-9 . The maximum deviation occurring in azimuth is about $.006^{\circ}$ and is not regarded as serious. It may be noted that the magnitudes of the changes in elevation bending due to the "Ottawa trough" are the same as those due to the use of simultaneous, separated radiosonde profiles for the same initial elevation angle at the surface.

iii) SECEDE III Refraction Experiment

During the barium release experiments conducted near Fairbanks, Alaska during March 1969, Lincoln participants recorded a number of UHF satellite tracks at Clear MEWS.

In subsequent analysis at Millstone, residuals are being determined relative to short orbital arcs fitted to two-second averages of the recorded raw observations. Some perturbations have been disclosed which may be tentatively attributed to natural aurora. Other perturbations noted appear to correspond with passage of the line of sight through ionized barium.

iv) Equatorial Scintillations

Millstone staff are also involved in work underway at Lincoln Laboratory to determine the magnitude angle-of-arrival fluctuations encountered by the Tradex radar on Kwajalein (Marshall Islands) when viewing objects (at night) through equatorial Spread F (Sec. 3). This phenomenon has most of the same characteristics as scintillation encountered in the auroral region and hence can serve as a useful model, yet there is no certainty that the magnitude of the effect will be the same in the two regions in view of the different geometry of the earth's magnetic field.

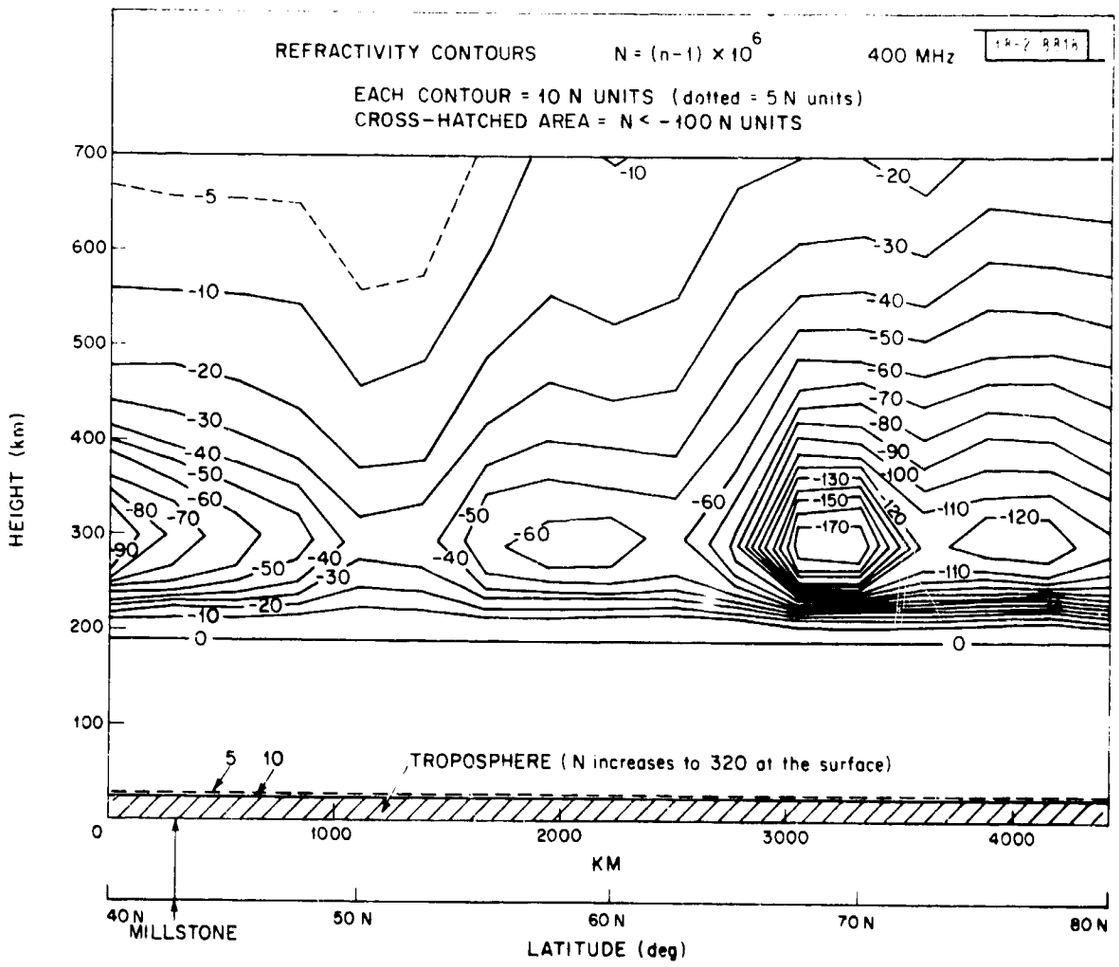

Fig. 5-8. Refractivity contours for F region as a function of latitude showing "Ottawa trough" of ion density.

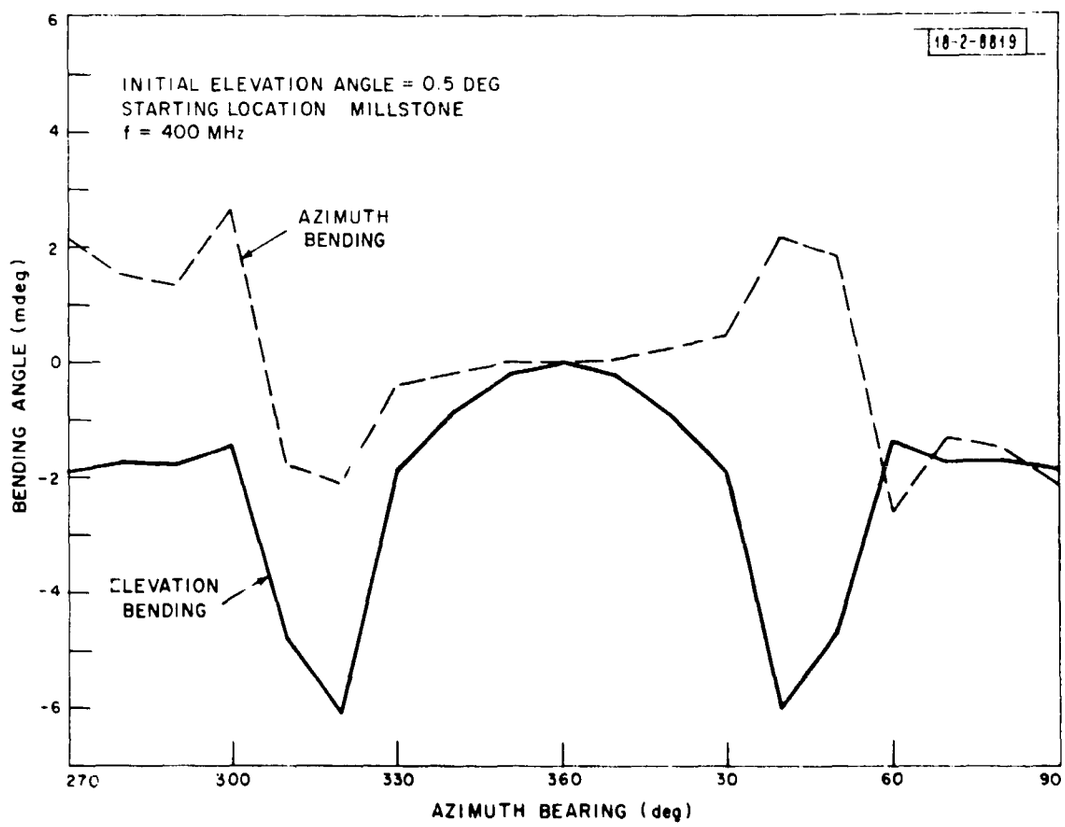

Fig. 5-9. Bending of a ray through Ottawa trough (Fig. 5-8) for initial elevation angle of 0.5°.

6. Auroral Studies

A. Introduction

The program of refraction measurements discussed in the previous section represents a new program of work. The auroral studies, however, are in part an extension of an earlier small program. The scientific results of this program have been published (Newell and Abel 1968; Abel and Newell 1969). In this earlier work radio auroral echoes observed during the afternoon period 1700-2100 were collected on 26 days during the period May 1965 to January 1966. It was found that the echoes were returned from a layer-like region having a thickness of 5-20 km and located at an average height near 110 km. The echoes were strongly aspect sensitive, and none were obtained from regions where the aspect angle was greater than about 3°. Both the occurrence of auroral echoes and the southernmost limit of the echo region were found to correlate with the magnetic index Kp. The Doppler spectra of the echoes showed predominantly approaching velocities to the east of the magnetic meridian and receding velocities to the west. The magnitude of the Doppler offset and the variation of offset with azimuth thus favored the two-stream plasma instability theory of Farley as an explanation of auroral echoes (Sec. 4 E). It was also suggested that the direction of plasma wave motion together with the variations of electrojet current with altitude may explain the presence of echoes at the magnetic meridian (not expected from the Farley theory for an east west current).

Further (unpublished) measurements were made during the period January-March 1968 mainly to test out possible programs for routine observations, and included samples on 8 days. Pulse lengths of 500, 100, 50 and 10 μsec were used. For various practical reasons the Doppler data could not be retrieved. The signal-to-noise ratios were considerably higher than those measured in 1965 and absolute volume reflectivity values were up to 20 db above previous values; calibration difficulties brought about essentially by the much stronger signal do not allow an exact comparison to be made. The strong signal also made the side-lobe effects much more in evidence in synthesized

range-height cross-sections. Beam-width pulse-length smearing was also evident as absolute reflectivity measurements made at 500 and 100 μsec in the same echo differed by up to 6 db. A complete stepped-scan was made with each pulse length in turn and the procedure repeated for eight hours so that this difference is not simply a consequence of time changes in the scattering volume.

While the pulse-length smearing may be reduced, albeit at the expense of Doppler information, the beam width influence remains. As a compromise the observation program presently being operated collects data at 500 and 50 μsec as described below.

In sum, as discussed in Section 4 radar auroral clutter is overwhelmingly under the control of the geometry of the magnetic field lines (Sec. 6 C). Thus to extrapolate the results obtained at Millstone to other geographic locations or operating frequencies requires a good theoretical understanding of the physics of the phenomenon, which currently is lacking. Our work to date supports the two-stream instability theory but in order to verify this model a complicated mix of parameters must be taken into consideration. These factors are discussed in the section that follows. The work that is being undertaken in the program is discussed in Section 6 C.

While special scientific interest is attached to obtaining a theoretical understanding of the aurora additional objectives of this program (discussed in Sec. 2 C) involve simply improving our knowledge of the morphology of the phenomenon both on finer distance and time scales, and a central objective is to determine if there is anomalous ionospheric refraction at times when auroral clutter echoes are present.

B. Test of the Two-Stream Instability Theory

i) General

If the theoretical interpretation discussed in Section 4 E is correct, then the radio auroral echoes may be treated as tracers of the E-region current distribution. This current distribution cannot be measured directly from the ground because magnetometer measurements are usually

dominated by the Hall current component. In order to provide a satisfactory interpretation of the observations it is desirable to have measurements of the various parameters involved in the theory, to construct a model of expected echoes based on the theories, and to compare the model and observations. This section will briefly summarize present information on the parameters used in the theory.

ii) Electron Concentration

Ground-based ionosondes give some information on the electron concentration profiles subject to the usual uncertainties of interpretation. There are few stations directly under the auroral electrojet. The critical frequency for sporadic E sometimes observed near strong electrojets may reach 10 MHz corresponding formally to concentrations of 10^6 cm^{-3}, but if the plasma waves themselves are responsible for the echoes, the usual relationship may not hold. The time variation of auroral E(s) fits very well with radio aurora and they may well be the same phenomenon. (Sec. 3).

A more effective procedure is to measure the auroral electron concentration by rockets, and Pfister (1964) has reviewed this topic. Concentrations in the vicinity of 110 km are in the 10^5 -10^6 cm^{-3} range. The variability is quite large and the question arises concerning the profile to be used in any model calculations. Two different sets were selected by Abel and Newell (1969) also Newell and Abel (1968) as a basis for conductivity computations. In addition to electron concentrations, collision frequencies and mean ionic mass are required. The standard formulae for the collision frequencies in turn require information about electron temperature and neutral particle concentration.

Three components of conductivity must be computed: along the magnetic field (longitudinal), along the applied electric field (Pederson), and along a perpendicular to both fields (Hall). The longitudinal component is always the largest, and electric field components along the magnetic field are thereby kept small. At about 110 km the Hall conductivity is largest (this is why a current flows towards the east in response to an electric field directed northwards) but by about 130 km and above the Pederson

conductivity dominates. The resulting current vector rotates anticlockwise with altitude (as viewed from above).

An unresolved question is the origin of the enhanced electron concentrations. During disturbed conditions the radio auroral echoes and current cores appear to move equatorward; concomitantly, plasma sheet electrons move towards lower L -values and judging by the resemblance between plasma sheet electron and precipitated auroral electron energy spectra it may be these particles that produce the enhanced conductivity.

It may be possible to judge the horizontal variations in concentrations from a measure of the input particle flux which then presumably governs this concentration. Possibilities for measuring this flux are outlined in Section C below. Production rate can be calculated from the flux using standard methods, but there is still a degree of uncertainty in the recombination processes which must be assumed before concentrations may be computed.

iii) Electric Field

Three methods have been used to derive the electric fields: direct measurement by rockets, measurement of the drift of ionized clouds at heights of under 200 km where both electron and ion drift is dominated by the field, and measurement of the field at balloon levels making use of the concept that this field is generally dominated by the field mapped down from the ionosphere. Values in the range 10-50 mv/meter are obtained and there is a field reversal from northwards to southwards near midnight consistent with what would be expected on the basis of magnetometer results (Figure 4-1).

The origin of the large scale magnetic field is thought to be plasma convective processes in the magnetosphere. In view of the capability to measure quite detailed velocity patterns in the radio aurora one might expect to learn more about the convection from the measurements. In particular one might take the various deductions concerning east-west currents and map the associated electric fields back to the magnetosphere. It is not known whether the fine structure observed in the electric field is due to conductivity and thence electron concentration structure, or some other effect.

In this connection more study is required of the mapping problem and this may be helpful also in connection with the origin of spread F. Possibly longitudinal electric fields accompanying the plasma waves in the E-region may be mapped up to the F-regions.

iv) Magnetic Field

The usual procedure is to extrapolate the surface magnetic field upwards to obtain the field at altitude (see Sec. 6 C), but this ignores perturbations introduced by local current systems. Potter and Cahill (1969) describe one such perturbation measured in an aurora. Further examination of the problem is required.

v) Particle Temperatures

Electron, ion, and neutral particle temperatures are required in any detailed comparison of results with models. Pfister (1967) has reviewed measurements of the electron temperature. Values in the range 500 - 2000°K at heights of about 110 km are reported, but there has been a very limited sampling. There appear to be no measurements of ion or neutral particle temperatures specifically made in auroras and values based on mean values for auroral latitude are used. The real neutral temperatures may be quite different as joule losses in the strong currents may provide heat energy as is probably reflected in changes in satellite drag observed at high Kp at levels above the auroral zone.

vi) Neutral Winds

The Kato and Farley theories assume the ions are at rest. As already noted electric fields invalidate this assumption at altitudes above about 110 km. Ion-neutral collisions will also transmit neutral particle motion to the ions in the E-region and the actual neutral wind distribution must be considered in any attempt to reconcile observed and theoretical Doppler velocity distributions. Meteor trails are tracked to provide neutral wind velocities at Durham, New Hampshire, Havana, Illinois, and Stanford. From the three stations a measure of the amplitude of the tidal components may be obtained that gives a first approximation to that expected over the auroral

zone. The smaller scale features cannot be determined in this way without more localized measurements. Little data has been circulated from these stations so far and it remains to see if the results are helpful in the present problem.

C. Future Work

i) Scientific Requirements

Doppler observations are required on a number of occasions so that syntheses such as that for November 5, 1965 may be attempted and the time evolution of the Doppler patterns may be followed. A reasonable first goal is 10 days with observations over at least a 12 hour period on each. The object is to obtain a better measure of the structure of the currents forming the auroral electrojet, and to see if the fields can be mapped to give information about magnetospheric convection.

The extent to which the observations may be explained by the two-stream theories is also of interest; there may be days of drifting irregularities which do not fit the theory as appears to be the case for the equatorial electrojet.

Intensity observations are also required during the period of the Active Sun for comparison with those made in 1965. Particular attention should be paid to the real scale sizes occurring and to possible correlations with incoming particle flux. A reasonable goal for this study is 20 days of more limited observations with a target of 5 days for radar-satellite comparisons. (See below) Based upon experience in 1965 20 days results would require about 40 days observations. A new data gathering scheme has been devised that will greatly assist the recovery of all the relevant radar information and is described below.

Finally for any periods of planned in-situ observations of the auroral electrojet at Fort Churchill an effort should be made to monitor the jet from Millstone. A comparison of the Doppler velocity observed should be made with local neutral wind velocities in the vicinity of 100 km altitude.

ii) The New-data Taking Procedure

For the most part, current theoretical models of radar aurora have drawn heavily upon observations taken with long integration times (Sec. 4). The on-line computer, together with the great sensitivity of the Millstone L-band radar, makes possible an investigation of echo behavior on a time scale of tens of milliseconds. To this end, the program for Short Time Analysis of Radar Echoes (STARE) was designed. It is hoped that such observations will give new insight into the physical mechanism of the scattering region.

The STARE program directs the antenna beam through a sequence of previously specified locations, and records a)echo power as a function of range, b)the echo spectrum as a function of range, and c)the operating characteristics of the radar. The data are stored on digital magnetic tape.

The basic scheme is to transmit alternately pulses of lengths of 50 and 500 μsec. The short pulse, with its intrinsic spectral width of 20 KHz, is used only for range resolution. The longer pulse, having a 2 KHz width, is used in conjunction with a comb of 24 matched filters. The bandwidth of the filter comb is 48 KHz, or 10 km/sec in terms of velocity (Doppler) spread. The repetition period for both pulses is 40 msec.

The effect in frequency of interruption of the transmission and the finite width of the matched filters is to smear over 2 KHz the true scattering function of the ionospheric irregularities. However, this function can be specified analytically and the spectral components passed by the system can be restored to their original strengths by post-processing. Some spectral components are, of course, lost irretrievably yet current observations include returns nearly 48 KHz in width, and thus the major features of the spectrum are being recorded.

A major problem to the STARE technique is data examination. At present, observations consisting of approximately 400,000 frames of data have been obtained where each frame occupies 80 msec of integration. We are

currently preparing to record existing data on 16 mm motion picture film. The plane of each frame will contain a 2-dimensional cartesian coordinate system of range and frequency. The echo-power of each range-frequency box will be density modulated. In this way, the data can be examined at a rate approximately twice that at which it was taken. Echo patterns of particular interest can be accessed from the original data tapes for quantitative analysis.

The STARE program may also be used for compiling data for 80 m.sec, and a considerable number of observations have been made in this mode. These observations employ integration times of 3 to 10 seconds and are employed to search for weak returns over wide ranges of sky.

iii) UHF Surveillance

The AN-FPS-35 surveillance radar at Montauk A.F.S. Long Island, New York will be used to obtain radar aurora backscatter data at a UHF frequency. The Montauk data will provide an indication of radar auroral activity during the satellite tracks at Millstone Hill radar.

When operated in its normal mode the FPS-35 has too high a PRF for auroral studies so the system requires a modification in order to obtain unambiguous backscatter data. The plan is to transmit every fifth pulse at an independent frequency and have a separate auroral receiver tuned to that frequency. The radar will be set up to operate in this mode only when the antenna is pointed in a 90 degree northern sector. The radar will transmit its normal pulsed F.M. signal all the time. With this mode of operating the radar will have a longer pulse that is not compressed. Small additional modifications will be required to obtain correct triggers and PPI scope sweeps for recording data. The data will be recorded by photographing a PPI scope display.

The preliminary investigation for the modification is complete and a detailed plan is in progress.

iv) Satellite Probing

a) The OV1-18 Satellite

In order to further our understanding of the physical nature of the aurora it would be invaluable to have information concerning a)the optical emissions accompanying the phenomenon b)the electric fields and conductivity in the auroral region and c)the energy spectrum of precipitating particles. These measurements can best be obtained using satellite sensors. Of various satellites now in orbit the Lockheed satellite, OV1-18, seems most suited to this task. This satellite has the characteristics given in Table 6-1 and is equipped with the instruments listed in Table 6-2.

b) Possible Contractual Arrangements with Lockheed Palo Alto Research Laboratory

An informal inquiry was made in November 1968 to the Lockheed Palo Alto Research Laboratory, Lockheed Missile & Space Company concerning their future programs for satellite observations of the properties of auroral particle precipitations and possible cooperation or collaboration with the UHF radio auroral studies under consideration at Millstone Hill. The utility of the OV1-18 satellite for our purposes was further investigated with the cooperation of Dr. R. G. Johnson of the Lockheed Laboratory by correspondence and a brief meeting in Washington, D. C. on April 24. Dr. Johnson has discussed the proposed coordination with Lt. Col. Lerohl, the ARPA program monitor for their contract and obtained an agreement that a coordinated program with the Millstone program represents a useful and suitable function for the satellite payload which consequently resulted in the inclusion of an option written into the OV1-18 Satellite Operations Document to operate the satellite payload in our area. During the period of coordination, it is anticipated that we would be provided with a map showing daily locations and lines of overpass in the Boston area updated weekly at no cost. The probable cost of evaluating data depends largely upon the extent and characteristics of the data.

c) Technical Goals and Considerations

The technical competence and interest of the Lockheed group is attested by previous publications and collaboration with radio observations of the auroral in Alaska by Stanford Research Institute (R. G. Johnson et al. 1967, Sharp and Johnson 1968). This satellite will orbit the auroral area under surveillance by Millstone at altitudes around 500 km, i.e. well above the altitudes giving rise to radio echoes at UHF. Despite this, when due consideration is made for the magnetic L shells, the results at the 500 km altitude should provide a detailed profile of a few kilometers resolution of the precipitating electron and proton energy spectrum of primary interest to radio observations of the aurora (Rees 1963). Although there is general agreement that the mechanism of auroral radar backscatter and perhaps radio scintillation phenomena require precipitating particles as a source the spatial location of the radio scattering irregularities is not necessarily determined directly by the regions of the particle precipitation on a fine-grained distribution. For these and similar reasons, it is expected that an exploratory series of the coordinated measurements will be undertaken during the regular operational auroral backscatter measurements at Millstone in the late summer or early fall of 1969. Depending upon the success in making simultaneous satellite and radar observations of auroral activity these preliminary measurements will be evaluated for possible continuation and more extensive data recovery and analysis requiring appropriate funding.

v) Field Orientation Computations

As noted in Sec. 4, both radar backscatter and bistatic reflection of radio signals from auroral zones require suitable orientation of the beam(s) with respect to the magnetic field lines The optimum geometrical situation for backscatter is given by

$$\cos \theta_1 + \cos \theta_2 = 0 \qquad (6\text{-}1)$$

where θ_1 and θ_2 are the angles between the propagation vectors and the magnetic field line at the backscatter center. The scattered power received decreases rapidly for angles which differ by only a few degrees from the ideal

TABLE 6-1

OV1-18 SATELLITE

Launch:	0748 U.T. March 18, 1969
Inclination:	98.9°
Perigee:	470 km
Apogee:	590 km
Period:	95.1 min
Operational Life:	~ 1 year
Data Acquisition Capability:	2 tape-recorded orbits per day

TABLE 6-2

INSTRUMENTATION ON OV1-18

I. Protons

A. Foil Threshold Detectors (Integral)

0°:	-,	9,	--,	38,	---	keV
55°:	3,	9,	26,	38,	500	keV
90°:	-,	9,	--,	38,	---	keV
180°:	-,	9,	26,	38,	500	keV

B. Differential Energy Intervals

55°: 1, 3, 8 keV (Velocity filter plus electrostatic analysis)

55°: 1, 3, 8 keV (Magnetic Deflection)

II. Electrons

A. Differential Energy Intervals (Magnetic Analysis)

0°:	1,	2,	5,	11,	24	keV
55°:	1,	2,	5,	11,	--	keV
90°:	1,	2,	5,	11,	--	keV
180°:	1,	3,	9,	27,	--	keV

B. Threshold Detector (Foils and Electrostatic)

0°:	0.2,	1.2,	--,	--,	--	keV
55°:	0.2,	1.2,	21,	--,	--	keV
90°:	0.2,	1.2,	3,	6,	40	keV
180°:	26,	--,	--,	--,	--	keV

III. Alpha Particles

55°: 1, 3, 8 keV (Velocity filter plus electrostatic analyzer)

TABLE 6-2 (Continued)

IV. UV Monitors

Broadband UV monitors are included at 55° and 180° to identify and correct for any UV background in the particle sensors.

V. High Energy Proton, Alpha Particle, and Electron Detector

Protons: 1 - 30 MeV

Alpha Particles: 7 - 20 MeV

Electrons: -.4 - 2 MeV

VI. Ion Energy Analyzer

Positive Ion Trap for ion density and temperature information.

VII. Epithermal Electron Analyzer

Retarding potential analyzer for electrons from 1 to 125 eV.

VIII. Langmuir Probe

Retarding potential probe for thermal electron density and temperature.

case. When the transmitter and receiver are at the same point, the maximum backscatter occurs when the propagation vector is perpendicular to the magnetic field vector at the point of reflection. To explain this aspect sensitivity it has been suggested that the reflection is caused by columns of ionized particles aligned along the field lines. Other explanations involving plasma instabilities have been put forth. It is, therefore, important to know the aspect angle, i.e., the angle between the propagation vector and the field line, as a function either of the scattering area's azimuth, elevation and range from the radar site or its longitude, latitude and height.

A general program called ASPECT has been written for the CDC-3300 computer in FORTRAN which computes the aspect angle as a function of two coordinate variables with the third held fixed when the transmitter and receiver are at the same location. The results are tabulated on the line printer and contour plots of constant aspect angle are drawn on the DD280 display unit. The program is intended to be more versatile than the available programs, and has four modes of operation for different coordinate displays

MODE 1: Aspect angle versus latitude and longitude for fixed height.

MODE 2: Aspect angle versus range and azimuth for fixed elevation.

MODE 3: Aspect angle versus elevation and azimuth for fixed height.

MODE 4: Aspect angle versus range and azimuth for fixed height.

The geometry of the problem is shown in Figure 6-1. In each mode the vectors P, Q, R and F are reduced to their cartesian components and the appropriate dot product taken.

There are two magnetic field models available in the program. One is a dipole field (subroutine MDIPOLE) which has its pole at $78^{\circ}.5$ north latitude and 69° west longitude. The other is a multipole field (subroutine FIELD) which uses the Hendricks and Cain multipole field coefficients.

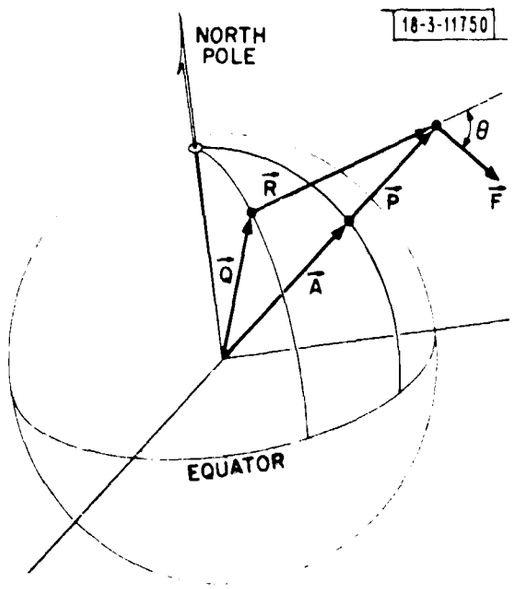

$\vec{Q}$ vector from center of earth to radar site

$\vec{R}$ vector from radar site to auroral reflection point

$\vec{F}$ magnetic field vector at reflection point

$\vec{P}$ vector from center of earth to reflection point

$\vec{A}$ vector from center of earth to subauroral point

$$\theta = \cos^{-1}\left|\frac{\vec{F}\cdot\vec{R}}{|F|\,|R|}\right| = \pm 90$$

Fig. 6-1. Geometry for determining ray direction $\vec{R}$ that is perpendicular to magnetic field vector $\vec{F}$.

This subroutine was supplied by L. Coury of IBM.[1] The field model has evolutionary terms and repudiatedly has an overall accuracy 1.5° in field orientation.

The program accounts for the ellipticity of the earth by using the standard ellipsoid model for its figure. Elevation angles are given with respect to a plane perpendicular to a line from the center of the earth. Refraction has not been taken into account. However, a refraction matrix, giving elevation corrections as a function of elevation and range and frequency can easily be inserted into the program. A sample of a contour plot of zero aspect angle for the Millstone Hill Radar is shown in Figure 6-2.

1. L. Coury, AFCRL Report 68-0046, "Program Solutions to Space Science Problems"

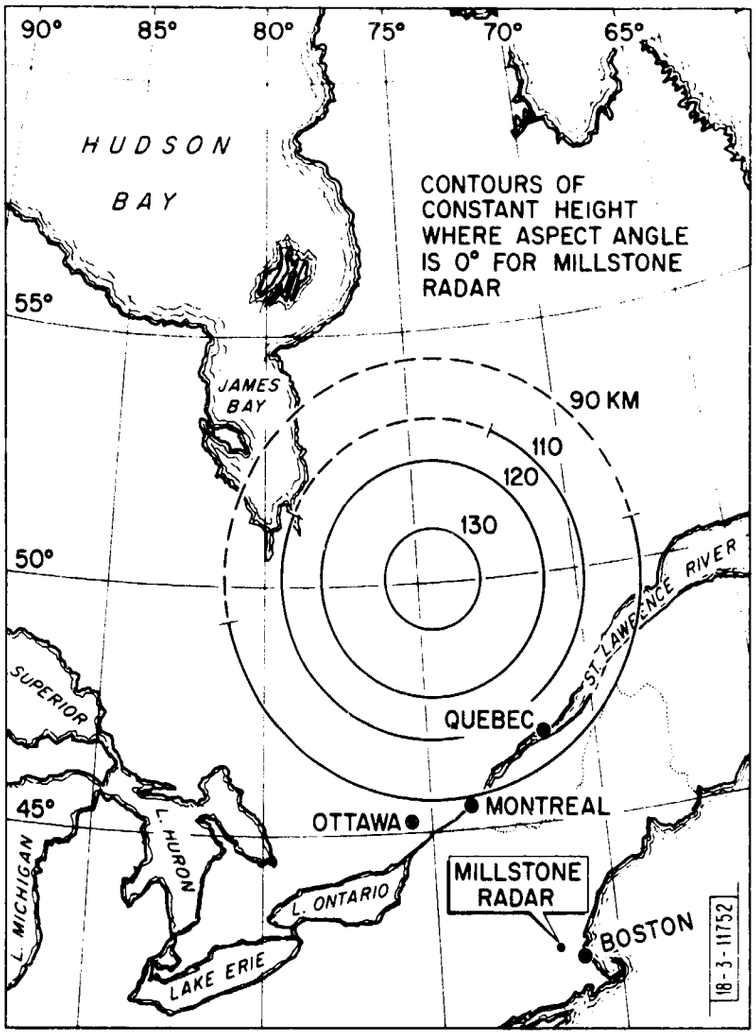

Fig. 6-2. Loci of perpendicular points from Millstone at various altitudes.

REFERENCES

W.G. Abel and R.E. Newell, J. Geophys. Res. 74, 231 (1969).

S.I. Akasofu, S. Chapman and C.I. Meng, J. Atmos. Terr. Phys. 27, 1295 (1965).

P.R. Arendt, A. Papayoanou and H. Soicher, Proc. IEEE 53, 268 (1965).

B.A. Bagaryatskii, Soviet Phys. Usp. 4, 70 (1961).

B.R. Bean and E.J. Dutton, "Radio Meteorology U.S. Govt. Printing Office Washington, D.C. (1966).

H.G. Booker, "Physics of the Upper Atmosphere", (Ed. J.A. Ratcliffe) Academic Press, N.Y. p. 355 (1960).

W.Calvert and C.W. Schmid, J. Geophys. Res. 69, 1839 (1964).

J.W. Chamberlain, Physics of the Aurora and Airglow", Academic Press, New York, p.232, (1961).

W.G. Chesnut, J.C. Hodges and R. Leadabrand, "Auroral Backscatter Wavelength Dependence Studies", Final Report AF 30(602)-3734, Stanford Research Institute, (1968).

T.J. Elkins, M.D. Papagiannis and J. Aarons, Space Res. VIII,p. 405 (1968).

C.D. Ellyett, J. Atmos. Terr. Phys. 31, 671 (1969).

J. V. Evans, Proc. IEEE 57, 496 (1969).

D. T. Farley Jr., J. Geophys. Res. 68, 6083 (1963).

P.A. Forsyth, Ann. de Geophys. 24, 555 (1968).

E.J. Fremouw and J.H. Lansinger, J. Geophys. Res. 73, 3053 (1968).

"Handbook of Geophysics", Revised Edition, Prepared for USAF Geophysics Research Directorate, Macmillan and Co., New York (1960).

T.R. Hartz, "Ionospheric Radio Communications", Plenum Press p. 9, (1968).

L.R. Hughes, J. H. Gibbs and L.A. Morgan, "Target Accuracy Experiment" Smyth Research Associates, San Diego, Calif. RADC-TDR-63-460 (U79 753A) (1964).

B. Hultiqvist and A. Egeland, Space Sci. Rev. 3, 27 (1964).

R.G. Johnson, R.E. Meyerott and J.E. Evans, "Aurora and Air Glow", (Ed. B. McCormack) Rheinhold Book Co. p. 169 (1967).

S. Kato and Y. Hirata, Dept. Ionos. Space Res. Japan, 21, 85 (1967).

H.G. Lange-Hesse, "Ionospheric Radio Communications", Plenum Press, p. 174, (1968).

R.S. Lawrence, C.G. Little and H.J.A. Chivers, Proc. IEEE 52, 4 (1964).

R.L. Leadabrand, J.C. Schlobohn and M.J. Baron, J. Geophys. Res. 70, 4235 (1965).

G.H. Millman, "Atmospheric and Extraterrestrial Effects on Radio Wave Propagation", General Electric Co., Syracuse New York TIS R61 EMH29 (1961).

R.E. Newell and W.G. Abel, Nature, 218, 454 (1968).

A. Nishida, J. Geophys. Res. 72, 6051 (1967).

W. Pfister, Space Sci. Revs. 7, 642 (1967).

W.F. Potter and L.J. Cahill, "Measurements near an Auroral Electrojet", Unpublished manuscript (1969).

M.H. Rees, Planet. Space Sci. 11, 1209 (1963).

T.F. Rogers and J.V. Evans, "Radar Astronomy", (Eds. J.V Evans and T. Hagfors) Ch. 2, McGraw Hill, New York (1968).

R.D. Sharp and R.G. Johnson, J. Geophys. Res. 73, 969 (1968).

E.K. Smith, "World Wide Occurrence of Sporadic E", NBS Circular 582, U.S. Govt. Printing Office, Washington D.C. (1957).

W. J. Stringer and A.E. Belon, J. Geophys. Res. 72, 4415 (1967).

M. Sugiura and J.T. Heppner, "Introduction to Space Science", (Ed. W.N. Hess) Gordon and Breach, New York, p. 5 (1965).

R.S. Unwin and F.B. Knox, J. Atmos. Terr. Phys. 30, 25 (1968).

A.L. Voronin, Geomag. and Aeron. 4, 421 (1964).

S. Weisbrod and L.J. Anderson, Proc. IRE 47, 1770 (1959) see also S. Weisbrod and L. Colin, Trans. IRE PGAP AP-8, 107 (1960).

UNCLASSIFIED
Security Classification

DOCUMENT CONTROL DATA – R&D

(Security classification of title, body of abstract and indexing annotation must be entered when the overall report is classified)

1. ORIGINATING ACTIVITY *(Corporate author)* Lincoln Laboratory, M.I.T.	2a. REPORT SECURITY CLASSIFICATION Unclassified 2b. GROUP None

3. REPORT TITLE

The Millstone Hill Propagation Study

4. DESCRIPTIVE NOTES *(Type of report and inclusive dates)*

Technical Note

5. AUTHOR(S) *(Last name, first name, initial)*

Evans, John V., Editor

6. REPORT DATE 26 September 1969	7a. TOTAL NO. OF PAGES 94	7b. NO. OF REFS 39
8a. CONTRACT OR GRANT NO. AF 19(628)-5167 b. PROJECT NO. 7X263304D215 c. d.	9a. ORIGINATOR'S REPORT NUMBER(S) Technical Note 1969-51 9b. OTHER REPORT NO(S) *(Any other numbers that may be assigned this report)* ESD-TR-69-306	

10. AVAILABILITY/LIMITATION NOTICES

This document has been approved for public release and sale; its distribution is unlimited.

11. SUPPLEMENTARY NOTES None	12. SPONSORING MILITARY ACTIVITY Office of the Chief of Research and Development, Department of the Army

13. ABSTRACT

Defensive radar systems for detecting and locating ballistic missiles must be designed to combat the degradation in system performance that can result from atmospheric and ionospheric refraction effects, clutter and scintillation. These phenomena become increasingly severe at low elevation angles and for high latitude stations there is a broad azimuthal sector where the effects are especially severe owing to the very irregular nature of the polar ionosphere and the presence of the aurora.

A program of measurements and data analysis is in progress, primarily centered at the Millstone Hill radar facility, designed to evaluate tropospheric and ionospheric effects on radar measurements capability, with emphasis upon disturbed ionospheric conditions (e.g., when radio aurora [illegible]). The work is being undertaken jointly by staff members of the Lincoln Laboratory and the Bell Telephone Laboratories. Emphasis in these measurements will be on attempting to separate and characterize the ionospheric and tropospheric components of refraction and scintillation. In order to do this, a UHF lobe-comparison satellite-beacon tracking capability is being added to the precise L-band tracking radar at Millstone. This will permit simultaneous dual-frequency measurements of angle-of-arrival, amplitude and phase fluctuations for paths traversing the polar ionosphere as well as in other directions less subject to propagation effects.

14. KEY WORDS

Millstone radar	ballistic missiles	clutter
propagation effects	atmospheric refraction	scintillation
UHF	ionospheric refraction	aurorae
radar measurements	tropospheric effects	L-band
satellite tracking		

UNCLASSIFIED
Security Classification